



TITLE:

Global Bifurcation Structure in Periodically Stimulated Giant Axons of Squid(Mathematical Topics in Biology)

AUTHOR(S):

Hanyu, Yoshiro; Takahashi, Nobuyuki; Musha, Toshimitsu; Kubo, Ryogo; Matsumoto, Gen

CITATION:

Hanyu, Yoshiro ...[et al]. Global Bifurcation Structure in Periodically Stimulated Giant Axons of Squid(Mathematical Topics in Biology). 数理解析研究所講究録 1989, 678: 276-324

ISSUE DATE:

1989-02

URL:

<http://hdl.handle.net/2433/101034>

RIGHT:

Global Bifurcation Structure
in
Periodically Stimulated Giant Axons of Squid

Yoshiro Hanyu* , Nobuyuki Takahashi**°,
Toshimitsu Musha**, Ryogo Kubo* and Gen Matsumoto+

* Department of Physics, Faculty of Science and Technology
Keio University
3-14-1 Hiyoshi, Kohoku-ku, Yokohama City, Kanagawa 223
Japan

** The Graduate School at Nagatsuda
Tokyo Institute of Technology
4259 Nagatsuda, Midori-ku, Yokohama City, Kanagawa 227
Japan

+ Electrotechnical Laboratory, Section of Molecular
and Cellular Neuroscience
Tsukuba City, Ibaraki 305
Japan

Please address all correspondence to Dr. Gen Matsumoto, Electrotechnical
Laboratory, Tsukuba City, Ibaraki 305, Japan.

° Present address: Department of Electrical Engineering, Faculty of
Engineering, Kyoto University, Yoshidahon Machi, Sakyo-ku, Kyoto City,
Kyoto 606, Japan.

+ to whom correspondence should be addressed.

Abstract

Potential responses of a squid giant axon under normal physiological environments were experimentally studied when the axon was stimulated by a train of periodic current pulses. The responses fell into three categories; phase-locked, quasi-periodic and chaotic. A bifurcation structure of the response patterns was obtained as a function of two bifurcation parameters, I/I_t (the current pulse intensity normalized by threshold current) and T (current pulse intervals). It was found that the firing rate in the periodic response changed in a stepwise fashion as a function of I/I_t or T and took a limited number of the Farrey series. In other words, the firing rate does not entirely take the form of a Cantor function. Furthermore, scaling properties were found in a series of the bifurcation parameter $(I/I_t)_n$ above which the firing rate of a periodic response was kept constant until the other mode of the response appeared. By comparing the experimentally determined scaling coefficients with those theoretically obtained for the map, $x_{n+1} = x_n + \varepsilon + A x_n^2$, by Kaneko (Prog.Theor.Phys. 69 (1983) 403), it was found that the periodic responses appeared through either the tangent bifurcation or the type III bifurcation, dependent on the bifurcation parameters of I/I_t and T . Presence of chaos in the response pattern in a limited region of the bifurcation parameters is a peculiar characteristic. The intermittent chaos appeared through the type III bifurcation, indicating that the bifurcation structure is homologous between both some parameter regions of the periodic response and the region of the intermittent chaos. These characteristics of the response patterns and the bifurcation structure could be qualitatively explained by considering double effects of periodic current input on normal axons; one is to exert as a periodic external force and the other is to induce the self-oscillation that the axon inherently retains. Both response and bifurcation

characteristics could be ascribed to a specific nonlinear interaction between the induced self-oscillation and the periodic input.

Introduction

Nonlinear and nonequilibrium oscillatory systems have exhibited phase-locking, quasiperiodic and chaotic behaviors when they are periodically driven. The systems well studied to date are the Rayleigh-Benard convection system^{1,2}, the barium-sodium-niobate (BSN) conductor³, the physical system of the charge density wave⁴, the Belusov-Zhabotinsky reaction system^{5,6}, the chicken heart⁷, the squid giant axon⁸ and so on. The phenomena found in these varieties of inherently oscillatory and externally periodically driven systems shared some commonality so that some physical properties could be reduced to a universal function⁹.

It has been suggested that squid giant axons are understood as a nonlinear and nonequilibrium system and that nerve excitation (impulse production) is grasped as a transition from a fixed point (the resting state) to a limit cycle (the repetitive firing state), assisted by an outwardly directed current stimulation¹⁰. In order to study the dynamic structure of the squid axon in more detail from a physical viewpoint, we have long been engaged in studying potential response characteristics of spontaneously repetitive firing axon to the periodic current stimulation and found that the response characteristics are quite analogous to those of other physical systems with inherent rhythm which are subject to periodic stimuli^{11,12}; three types of responses (phase-locked, quasi-periodic and chaotic responses) and also three kinds of route to the chaos (successive period-doubling, intermittency and collapse of the quasiperiodicity) were found. At the same time, chaotic potential responses to periodic current pulse inputs have been observed recently in normal (quiescent) squid giant axons under normal physiological conditions bathed in natural sea water^{13,14}.

The present paper is intended to describe a global bifurcation structure in periodically stimulated giant axons of squid to obtain a deeper physical insight.

to electrical excitation. The bifurcation structure observed here is compared with those of other physical and chemical nonlinear systems.

Materials and Methods

Materials Experiments were performed on isolated giant axons of squid (*Doryteuthis bleekeri*), captured in Sagami Bay and maintained in a special aquarium tank in the Electrotechnical Laboratory at Tsukuba City^{15,16,17}. Each giant axon, 400 - 600 μm in diameter and 60 - 80 mm in length, was carefully resected under a dissecting microscope. The axon thus prepared was placed in a chamber filled with natural seawater (NSW). The temperature of the axon was kept constant by controlling the temperature of the chamber within $\pm 0.1^\circ\text{C}$ in the temperature range 4 through 18°C .

Experimental procedures In order to monitor the electrophysiological responses of the axon, membrane potentials were measured at two locations independently; one (R_2) was placed to measure the membrane potential at the current stimulation site and the other (R_3) was placed to measure it about 30 mm away from the stimulation site (Fig.1). For this, we inserted two potential electrodes, R_2 and R_3 (glass pipette electrodes of the Ag - AgCl type, filled with 0.6 M KCl solution), inside the axon from the ends cut open on both sides, respectively. A reference potential electrode (R_1) bathed in NSW was used to give the reference potential for both these two internal potential electrodes.

The current stimulation was delivered through an internal current electrode (S) which was electrically connected to a pulse generator (Nihon-Koden Co. Ltd., type SEN 7103) through a 470 k Ω resistor. The current electrode was made of platinized-platinum wire of 5 mm in length. In order to measure the potential response characteristics of the axon to the periodic current stimulation, a train of periodic current pulses was delivered, where the pulse width was fixed at 300 μsec but the pulse intensity I and the time interval between neighbouring pulses T were changed as bifurcation parameters. In order to avoid axon fatigue, the number of current pulses involved in a single train

for one trial of the experiments was limited to 500 or less. There was a two-minute rest period after each train of periodic current pulses had stimulated the axon. After the rest, the resting potential usually recovered to the initial (or control) level. If the resting potential was not recovered or when the total number of current pulses given to an axon exceeded 30,000, we stopped using the axon for the experiments. Under these experimental conditions, the experiments could be stably performed for axons of $>450\ \mu\text{m}$ in diameter until 30,000 current pulses had been administered. This may have been because these axons possessed large buffering capacities against electrolysis accompanied by current stimulation¹⁸.

The external Ag - AgCl wire coil of $200\ \mu\text{m}$ in diameter and 12 mm in coil length (G) was placed in the chamber 51 mm wide, in parallel with the longitudinal direction of the axon, in order to ground the NSW.

Response pattern classification and data analysis Nonpropagating and propagating potential responses of the giant axon to periodic current pulse stimulations were obtained by the experimental procedures described above. Three typical experiments are illustrated in Fig.2, where the current intensity, I , of periodic stimulation pulses was a constant 1.5 times the current threshold, I_t , while the time interval, T , between adjacent pulses was changed; 6.4, 6.2 and 5.6 msec for records A, B and C, respectively. I_t was obtained experimentally as the pulse intensity just enough to evoke the action potential when a single current pulse was applied. In record A, obtained when T was 6.4 msec (longer than a refractory period^{18,19,20}), it is seen in the figure that one impulse regularly corresponds to one current pulse whether it is nonpropagating or propagating. This does not hold in records B and C. In record B, obtained when T was 6.2 msec, a pattern of the potential response is periodically repeated such that nine impulses are produced in succession and then one impulse is missed. This is caused by the refractory effect. A similar response is observed in record C

obtained when T was 5.6 msec. In record C, the pattern is qualitatively the same as that observed in record B but its period is shorter; that is, two impulses are evoked in succession and then one is missed. In order to characterize these response patterns, we adopted a notation originally developed by Harmon²¹: $1^m 0^n$ denotes a periodic sequence of firing pulses in which 0 (failure of action potential production by current pulse stimulation) appears consecutively n times after 1 (presence of action potential) has appeared consecutively m times. According to this notation, each periodic firing pattern in Fig.2 is 1 (record A), $1^9 0$ (record B) and $1^2 0$ (record C), respectively. An alternative notation to characterize response patterns is the firing rate, $m/(m+n)$, defined as m impulses produced by $(m+n)$ current pulses when the number of $(m+n)$ is quite large. The firing rate can be conveniently used to characterize not only periodic but also aperiodic potential responses, while the notation $1^m 0^n$ can only be used for periodic potential responses. For the responses of Fig.2, the firing rates are 1 (record A), $9/10$ (record B) and $2/3$ (record C), respectively.

In order to analyze these potential responses in more detail, we have developed two simple but effective methods: one of the methods is to measure latency, τ_n , between a current pulse and the impulse evoked by it, in succession (see upper *inset* of Fig.3), and to obtain τ_n as a function of the impulse sequence number n . Typical examples of these analyses are illustrated in records A, B and C of Fig.3, whose representative samples of potential responses were shown in records A, B and C of Fig.2, respectively. In record A, it is clear that τ_n 's are unchanged for all n . This means that this periodic potential response of firing pattern 1 is phase-locked. For firing pattern $1^9 0$, it is easily seen in record B of Fig.3 that this periodic response is also phase-locked. However, the response of the firing pattern $1^2 0$ does not retain the simple periodicity of 110 . This can be seen in record C of Fig.3 where τ_n 's are constant for odd numbers of n but those for the even numbers are frequency-modulated as a function of n . This

indicates that the response is quasi-periodic. The quasi-periodicity of the response could be further confirmed by plotting the τ_{n+2} vs. τ_n (Fig.4-1) or by obtaining frequency spectra calculated by the maximum entropy method (MEM) (Fig.4-2). The MEM was developed by Burg²² in 1967 to calculate frequency spectra from limited temporal data, by maximizing the information entropy, more precisely than those obtained by conventional methods. In Fig.4, the quasi-periodicity is characterized by the formation of a closed circle of data points in the τ_{n+2} vs. τ_n relation (Record 1) and, at the same time, by the appearance of shoulders around central peaks in the power spectral density (Record 2). The frequency difference between the center and shoulder of the spectra corresponds to the modulation frequency.

The other method of analyzing the temporal patterns of potential responses is to measure time intervals, t_n , between neighbouring impulses (see upper *inset* Fig.5), and to plot a diagram of the t_n -versus- n . Typical examples of these are illustrated in records A, B and C of Fig.5, where the data of temporal potential responses used for these analyses were the same as those used for obtaining records A, B and C of Fig.3, respectively. From these records, it is clear that the response patterns of 1 and 1⁹⁰ are both phase-locked (records A and B) but that the pattern of 1²⁰ is not phase-locked (record C). For the analysis of periodic or quasi-periodic patterns, it is well understood, by comparing the results of the τ_n vs. n (records of Fig.3) with those of the t_n vs. n (records of Fig.5), that the former analysis provides greater insight into detailed characteristics of the pattern than the latter one. One of the advantages of the former analysis is demonstrated in Fig.3C, where the modulation is clearly visible only in τ_n 's with even numbers of n , while it was weakly visible in t_n 's with both odd and even numbers in Fig.5C. However, for the analysis of aperiodic patterns where it is often difficult to define τ_n , the latter analysis will give us additional information on response characteristics.

Results

Global bifurcation diagram for patterns of firing potential responses

Potential responses of the squid giant axon to a train of periodic current pulses were experimentally studied to determine the bifurcation structure of the response pattern as a function of two bifurcation parameters, I/I_t and T . In the experiments, the isolated axon was bathed in NSW at 14°C and stimulated with periodic current pulses of I/I_t between 1 and 2.1 with a minimum step of 0.001 and of T between 2.6 and 6.5 msec with a step of 0.1 msec. For each measurement, I/I_t was first changed (increased and/or decreased between 1 and 2.1) while T was fixed at a given value. This experimental procedure was then repeated when T was reset, for the same (or different if necessary) axon.

Periodic and aperiodic firing responses were found^{13,14}. The global bifurcation diagram of the firing pattern thus obtained is illustrated in Fig.6 as a function of two dimensional bifurcation parameters, I/I_{th} and T , where periodic firing responses of types 1, 1^m0 ($m = 1, 2, \dots, 11$), and $(10)^{n-1}100$ ($n = 1, 2, \dots, 12$) were observed with chaotic firing responses (dotted parameter regions). The notation 0 in the diagram represents a region where no firing response was observed after only a single impulse response to the first pulse in a train of periodic current pulses. Periodic firing responses of the type 1^m0 were found in the bifurcation parameter region with large T (over 5 msec); that is, the firing patterns found in right half of the diagram. In this parameter region, the firing pattern 1^m0 rather abruptly bifurcated to the $1^{m+1}0$ pattern as I/I_t was increased with a fixed T or vice versa (i.e. when T was changed for a fixed I/I_t), until the 1 pattern emerged. Therefore, we can identify this parameter region as one involving firing patterns of a simple period-adding sequence or a period-adding sequence region. The detailed bifurcation characteristics between the 1^m0 and $1^{m+1}0$ patterns in *Region I* will be analyzed below.

The periodic firing responses of the type $(10)^{n-1}100$ were found when T was small (less than 3.0 msec) but I/I_t was large (larger than 1.7); that is, these types of responses are observed in the upper left of the bifurcation diagram. In this case, the firing pattern $(10)^{n-1}100$ also rather abruptly bifurcated to the pattern $(10)^n100$ with the increase of I/I_t and T . We identified this region as one involving firing patterns of a period-adding sequence or simply a period-adding sequence region. The detailed bifurcation characteristics in *Region II* will be also analyzed below.

Two different characteristics of chaotic firing responses were found. One is between the $(10)^{n-1}100$ and $(10)^n100$ firing patterns (band regions with random dots in the diagram), where $n = 1, 2, 3$ and 4 , when T was small (smaller than 4 msec) but I/I_t was intermediate (less than 1.7); that is, this region (*Region III*) is visible in the lower half of the bifurcation diagram as bands. It is seen that the bandwidth becomes narrower as n increases and is clearly discernible in the region between the $(10)^{n-1}100$ and $(10)^n100$ patterns for n of 1, 2, 3 and 4 in the experiments. Thus we refer to these regions alternating between chaotic and periodic patterns as functions of I/I_t and/or T . We will study the detailed bifurcation characteristics of these regions in *Region III* below. The other type of chaotic response patterns was found between the 10 and 0 responses when T was large (larger than 3.8 msec) but I/I_t was small (smaller than 1.25), as shown as the band (with regular dots) in the bifurcation diagram. When T and/or I/I_t decreased, chaotic responses in this band bifurcated to other chaotic ones until the 0 response pattern appeared. Therefore, we call this the continuous chaotic sequence region. The bifurcation characteristics in *Region IV* will be described below.

Detailed bifurcation characteristics

Region I (the simple period-adding sequence region)

Firing rates of the 1^{n0}

firing responses changed in a stepwise fashion as a function of the bifurcation parameters, I/I_t and T . A typical experiment is illustrated in Fig. 7A, where I/I_t changed from 1.0 through 2.1 while T was fixed at 5.0 msec. As I/I_t increased, it is seen in the figure that the firing rate, $n/(n+1)$, of the 1^{n0} response was unchanged for certain values of I/I_t , forming a plateau, until it changed abruptly to $(n+1)/(n+2)$ at a critical value of $(I/I_t)_{n+1}$. In order to investigate the bifurcation structure, particular attention was paid to firing response behaviors around the critical point of $(I/I_t)_{n+1}$. Figure 7B shows the behaviors at the critical points, with a control response of the 10 pattern (record a) when applied to the τ_n vs. n relations. Records b through f were obtained from non-propagating potential responses for I/I_t of 1.75 (b), 1.76 (c), 1.86 (d), 1.87 (e) and 1.96 (f), respectively. Among these values of I/I_t , critical values of $(I/I_t)_2$, $(I/I_t)_3$ and $(I/I_t)_8$ were 1.76, 1.87 and 1.96, respectively. In the transition between the 10 and 1^{20} responses, we cannot see any critical behaviors in the potential responses; that is, the 10 response at I/I_t of 1.75 does not contain any critical behavior as far as the τ_n vs. n relation is concerned (b), and is unchanged compared with the control at I/I_t of 1.43 (a). At the same time, the 1^{20} response at I/I_t of 1.76 (c) does not show any critical behavior either, since the τ_n obtained here oscillated regularly against n at a period of 2 (c). By analyzing the τ_n vs. n for potential responses at I/I_t of 1.86 (d) and 1.87 (e), we did not see any critical behaviors, within the experimental accuracy, in the transition between the 1^{20} and 1^{30} states either. This also holds for the transition behavior from the 1^{80} response (see record f). It is noted that τ_n s in records, d, e and f, oscillate regularly against n at periods of 2, 3 and 8, respectively. These indicate that the periodic firing responses of the 1^{n0} patterns are phase-locked, and that the phase-locking is well preserved even in the vicinity of transitions between the 1^{n0} and 1^{n+10} responses.

These structural analyses of the bifurcation characteristics were similarly performed in Region I for different T s. The above conclusions, that the 1^{n0} responses are periodic and phase-locked for all I/I_t when T was fixed, were further confirmed as T increased to 6.5 msec, except those responses observed for T around 6.0 msec (Fig.8).

Figure 8 shows the firing rate of nonpropagating potential responses as a function of I/I_t (Fig.8A) which were obtained as I/I_t changed from 1 through 2.1 while T was fixed at 6.0 msec, and the τ_n vs. n relations (Fig.8B) for six representative responses. It should be noted in Fig.8A that, at two values of I/I_t , a and b, the firing rate takes intermediate values between $1/2$ (corresponding to the 1^0 response) and $2/3$ (corresponding to the 1^{20} response) although, with these exceptions, it changes with I/I_t in a stepwise fashion. The τ_n vs. n analysis on the responses for a and b revealed that the 1^{20} response, which initially appeared on application of a train of periodic current pulses, became more and more unstable as the number of current pulses increased until finally the 1^0 response stably appeared (see records a and b in Fig.8B). When the 1^{20} response was still preserved, τ_n with even numbers n (upper branches of τ_n in records a and b) was frequency-modulated with n . It is clearly seen in records a to e that the modulation amplitude becomes smaller and, at the same time, the lasting number of even n increases as the 1^{20} responses become more stable. Lack of stability in the 1^{20} response with the stimulation number can be also characterized by delaying τ_n with n ; more rapidly the upper branch of τ_n is delayed in records a and b compared with records c and d (Fig.8B). Based on these considerations, the firing responses at I/I_t of c through d, which are classified as the 1^{20} responses (see Fig.8A), might transform to stable 1^0 responses with further stimulation. However, the 1^{20} response at I/I_t of e looks extremely stable as estimated from the stability criteria of the τ_n vs. n analysis. However, the 1^{30} response at I/I_t of f, which was classified after 375 current pulses were

given, might transit to stable 1^20 response if we continued stimulation. This indicates that, even if the periodic but phase-unlocked $1^{n+1}0$ response emerges initially, it will finally transform to a stable phase-locked 1^n0 response.

However, we observed that the phase-unlocked 1^20 response was steady when periodic current pulses with T of 5.6 msec and I/I_t of 1.5 were given (see Fig.2).

In this case, the response was classified into the quasi-periodic 1^20 pattern (Figs.3 and 4). This can be identified as the stabilized 1^20 quasi-periodic pattern and those seen in records a to d in Fig.8 as transient 1^20 quasi-periodic patterns.

Region II (the period-adding sequence region)

This region was defined as the bifurcation parameter region where only $(10)^{n-1}100$ responses ($n = 1, 2, 3, \dots, 12$) were elicited; that is, the region in the bifurcation diagram (Fig.6) surrounded by I/I_t larger than 1.25 and T smaller than 2.8 msec. The firing rate of the $(10)^{n-1}100$ response changed to that of the $(10)^n100$ one in a stepwise fashion as a function of the bifurcation parameters, I/I_t and T . A typical experiment showing this is illustrated in Figs.9A and 10A, where I/I_t was changed and T was fixed at 2.6 and 2.8 msec, respectively. It is seen in these figures that the firing rate, $n/(2n+1)$, of the $(10)^{n-1}100$ response was unchanged for certain values of I/I_t , forming a plateau, until it changed abruptly to $(n+1)/(2n+3)$ at a critical value of $(I/I_t)_n$. The detailed bifurcation characteristics were further investigated both by the τ_n vs. n analysis (Figs.9B and 10B) and by calculating the MEM power spectral density (Fig.11). Particular attention was paid to firing response behaviors around the critical point of $(I/I_t)_n$. Some of the transitional behaviors of responses obtained for T of 2.6 msec are shown in Figs.9B and 11A: For the transition between 100 and 10100 responses, even the 100 response just below point a was quite stable and phase-locked (record a in Fig.9B) but the 10100 response just above $(I/I_t)_2$ was steady but phase-unlocked; that is, quasi-periodic (record b in Fig.9B). The quasi-periodicity can be also confirmed by the MEM spectral analysis (record b

in Fig.11A). It was observed that the quasi-periodic character of the 10100 response was still preserved in the response observed at c away from the critical point of $(I/I_t)_2$, although the modulation frequencies in the upper branches of τ_n with n were found to be higher than those at b (compare records c with b in both Figs.9B and 11A). For the transition between the 10100 and $(10)^2100$ responses, responses in both patterns in the vicinity of the critical point of $(I/I_t)_3$ were quasi-periodic (records d and e in Figs.9B and 11A). This was also true for the $(10)^3100$ response for the transition between the $(10)^2100$ and $(10)^3100$ responses (record f in Fig.9). By contrast, the $(10)^{n-1}100$ responses obtained for T of 2.8 msec were all found to be phase-locked, even in the transitional regions of responses (see Figs.10B and 11B). Therefore, as T increases while I/I_t is fixed at a definite value larger than 1.25, the quasi-periodic $(10)^{n-1}100$ response, where $n = 2, 3, \dots, 12$, bifurcates to the phase-locked one at a critical value of T, T_c . Furthermore, it can be expected that the transition takes place at T_c simultaneously for all $(10)^{n-1}100$ responses. As T increases further, chaotic responses appear between the $(10)^{n-1}100$ and $(10)^n100$ responses ($n = 1, 2, 3, \dots$), as will be shown below.

Region III (the region alternating between chaotic and periodic responses)

This region was defined as the bifurcation parameter region where chaotic and periodic $(10)^{n-1}100$ responses were alternately elicited as a function of the bifurcation parameters; that is, the region in the bifurcation diagram (Fig.6) surrounded by I/I_t between 1.75 and 1.3 and by T between 3.0 and 3.8 msec. Firing rates of the periodic $(10)^{n-1}100$ response were $n/(2n+1)$ but those of chaotic responses changed continuously to exhibit a minimum between the $(10)^{n-1}100$ and $(10)^n100$ responses, where $n = 1, 2, 3, \dots$, as a function of I/I_t when T was fixed. A typical experiment for this is illustrated in Fig.12, where T was 3.8 msec and I/I_t changed from 1.0 through 2.1. Detailed structures of responses obtained for different I/I_t but common T of 3.8 msec were further studied by analyzing their

respective t_n vs. n relation (see Fig.5), as shown in Fig.13. Records a through o of Fig.13 correspond to responses with the firing rates of a through o in Fig.12, respectively. The t_n vs. n analysis showed that the 100 response was phase-locked at a but period-doubled at b. Further increase of I/I_t brought about long-lasting nonfiring periods intermittently, as seen in records c, d and e of Fig.13. Each nonfiring period of time was equally close to $5T$ for c and d, and frequencies of the nonfiring period increased with I/I_t . Prior to the intermittent nonfirings, the period-doubling was observed to be always unstable.

A further increase of I/I_t caused both nonfiring periods to become longer and more frequent. In record e, obtained from the response with the minimum firing rate (see Fig.12), nonfiring periods of $5T$, $6T$, $7T$ and $8T$, except for only one at $4T$, are frequent. It is noted in records c and d that the phase-locked 100 response was stabilized after the intermittent nonfiring bursts. However, in record e, the intermittent bursts and the 100 period-doubling responses coexisted during the time period of the experimental observation. Thus, the chaos emerging here as I/I_t increased was caused by disrupting unstabilized period-doubling 100 responses by intermittent nonfiring. Therefore, the bifurcation to the type III intermittent chaos²³ can be classified as a subcritical period-doubling bifurcation^{24,25,26}.

As I/I_t increased beyond the minimum firing rate, the 10100 response transiently appeared at early parts of the responses, followed by responses period-doubling 100 responses alternating with intermittent nonfiring bursts (f and g). In other words, the same characteristic of chaos as observed at e appeared after the 10100 response became unstable. The tendency of the instability was observed even at h (see record h). For I/I_t between h and i, the phase-locked 10100 response was observed to be quite stable. At i, the 10100 response was initially period-doubled but finally phase-locked (record i). Then, the firing rate again took a minimum between the 10100 and $(10)^2100$ responses (see

Fig.12). Accordingly, long-lasting periods of nonfiring appeared intermittently, followed by period-doubling instability of the 10100 response (records j and k). Therefore the chaos also appeared through the subcritical period-doubling bifurcation. At 1, the phase-locked $(10)^2100$ response emerged although it was initially period-doubled. It is seen in record m that the $(10)^3100$ response appeared initially, followed by the $(10)^2100$ intermittent chaos. Finally, the stable 10 response appeared for I/I_t larger than that at 0 (see record o), through complicated responses temporarily mixed with multipatterns of chaotic and periodic responses (record n).

All these indicate that the route to the chaos observed in Region III is commonly through the subcritical period-doubling bifurcation.

Region IV (the region with continuous chaotic sequence) This region was defined as the bifurcation parameter region where chaotic responses were observed between the 10 and 0 responses, that is, the region surrounded by T larger than 3.8 msec and I/I_t smaller than 1.4. Firing rates of chaotic responses changed continuously between 0 (the 0 response) and 0.5 (the 10 response) as a function of I/I_t (Fig.14A), where T was 4.0 msec. The t_n vs. n analysis revealed that the chaos observed here appeared by interrupting the 10 responses with long-lasting nonfiring intermittent periods (records b through c). In other words, the 10 phase-locked response (record f) bifurcated to intermittent chaotic responses (records a through e) until the 0 response appeared.

Scaling properties of the firing rate as a function of the bifurcation

parameter I/I_t In Region I, we observed that the 1^n0 response changed abruptly to the $1^{n+1}0$ response at a critical value of $(I/I_t)_{n+1}$ when T was fixed. As a result, we got a series of critical values, for two of which the firing rate was kept constant; $(I/I_t)_1, (I/I_t)_2, \dots, (I/I_t)_{11}, \dots, (I/I_t)_\infty$, where $(I/I_t)_\infty$ corresponds to the value above which the 1 response appears. Using these experimental

observables of $(I/I_t)_n$ and $(I/I_t)_\infty$, we found that $[(I/I_t)_\infty - (I/I_t)_n]$ as a function of n exhibited a scaling property expressed as $n^{-\lambda}$, where λ was found to be 1.8 for T of 5.0 msec and 2.0 for T of 6.0 and 6.5 msec, respectively (Fig.15).

The scaling property was similarly found in Region II, where the $(10)^{n-1}100$ response changed abruptly to the $(10)^n100$ response at a critical value of $(I/I_t)_n$. We found that $[(I/I_t)_\infty - (I/I_t)_n]$ had a scaling property of $n^{-\lambda}$, where λ was found to be 1.2 for T of 2.6 msec and 1.3 for T of 2.8 msec, respectively (Fig.16). It is noted that $(I/I_t)_\infty$ in this case corresponded to the critical value of I/I_t above which the 10 response appeared.

Discussion

In the present experiment, it was found that potential responses of the squid giant axon under normal physiological environments to periodically stimulated current pulses fell into three categories : (1) phase-locked, (2) quasi-periodic and (3) chaotic responses. A global response diagram was obtained as a function of two bifurcation parameters, I/I_t and T , as shown in Fig.6. As a result, two-dimensional bifurcation structures of the response were studied in detail. In the study, it was found that the periodic response was limited to two firing types; the $1^n 0$ and $(10)^{n-1} 100$ responses, where $n = 1, 2, 3, \dots, \infty$. The non-firing response (the 0 response) was the only exception. Furthermore, it was found that the firing rate took a limited number of the Farrey series (see Fig.17); 0 for the 0 response, $\frac{n}{n+1}$ for the $1^n 0$ response and $\frac{n}{2n+1}$ for the $(10)^{n-1} 100$ response. These results show that the stepwise change in the firing rate, as was theoretically predicted by Nagumo and his colleagues^{26,27} was experimentally confirmed in Regions I and II of the bifurcation diagram (Fig.6). However, it should be noted that the firing rate experimentally observed does not entirely take the form of an extended Cantor's function as theory would suggest^{27,28,29}.

The characteristics of Regions I and II could be also studied by our findings of the scaling law that governs both the bifurcation structure and the stepwise change in the firing rate :

$$\text{For Region I; } (I/I_t)_\infty - (I/I_t)_n \propto n^{-1.9} \dots\dots\dots(1),$$

and

$$\text{for Region II; } (I/I_t)_\infty - (I/I_t)_n \propto n^{-1.3} \dots\dots\dots(2),$$

where $(I/I_t)_n$ stands for a critical value of the normalized current pulse intensity above which the responses of $1^{n+1}0$ and $(10)^n 100$ appeared in Regions I and

II, respectively (see Figs.15 and 16). In other words, it was found that the scaling coefficients averaged 1.9 and 1.3 for the response with the simple period-adding sequence (Region I) and the period-adding sequence (Region II), respectively. The absolute values of the scaling exponents and the difference between those observed in Regions I and II may be basically explained according to the current theory of critical phenomena for the period-adding sequence of frequency-locked response developed by Kaneko^{30,31}. He studied its critical behavior with use of a one-dimensional map^{32,33}, as follows;

$$x_{n+1} = x_n + A \sin(2\pi x_n) + 0.25 \pmod{1} \dots\dots\dots(3).$$

His results can be summarized as follows. (1) Frequency locking states with rotation numbers of $n/(5n-1)$ appear in succession ($n = 1, 2, 3, \dots, \infty$) at A_n . (2) A scaling property that $A_\infty - A_n \propto n^{-2}$ was obtained and explained by the theory of intermittency^{34,35}. The same scaling property was obtained in a simulation of the Belousov-Zhabotinskii reaction³⁶. Since the locking occurs through a tangent bifurcation, the scaling property was generalized when a tangent bifurcation of the type $x_{n+1} = x_n + \varepsilon + A x_n^z \dots\dots\dots(4)$ (if $z=2$, this can be reduced to the above bifurcation type of eq.3) was introduced, followed by the result that

$$A_\infty - A_n \propto n^{-z/(z-1)} \dots\dots\dots(5).$$

The theoretically predicted value of the scaling coefficient 2 is very close to 1.9, the value obtained in Region I, for the simple period-adding bifurcation sequence. A typical example of eq.(4) has been observed in the simulation experiment of the Belousov-Zhabotinsky reaction³⁶. The excellent agreement suggests that the bifurcation between successive periodic orbits in Region I takes place tangentially.

However, in the case of the potential response with the period-adding bifurcation sequence (Region II), the scaling coefficient, 1.3, was experimentally obtained. This value could be close to 1.5, which corresponds to the case of $z=3$ in eq.(4). The difference between the experiment and the theory may be because the scaling law in the theory holds for sufficiently large numbers of n but the scaling coefficient was experimentally determined for definite numbers of n with maximum n of 11. The estimated coefficient value will tend to be smaller than the expected. These points indicate that the bifurcation mechanism is different between the simple period-adding sequence (Region I) and the period-adding one (Region II). Further, it is noted that the map, $x_{n+1} = x_n + \varepsilon + Ax_n^3$, leads to the type III bifurcation in the theory of intermittency^{23,34,35}. This is fully consistent with the fact that Region I neighbours Region III where the period-adding sequence bifurcates to an alternate sequence between chaos and phase locking, as shown in Fig.6. It was shown in *Results* that intermittent chaos appeared through the type III bifurcation in Region III. This means that the bifurcation structure is homologous both in Regions II and III while, in Region I, it appears through the tangent bifurcation.

These characteristics of both the response and the bifurcation could be compared with those experimentally observed in the system of the manganese-catalyzed Belusov-Zhabotinskii reaction in a stirred flow reactor by Maselko and Swinney^{5,6}. The similarities between their observations and ours are that (1) some states bifurcate in a staircase fashion, and that (2) both include period-adding and simple period-adding sequences. The differences are, however, that (1) any chaos is involved in their system, that (2) our periodic sequences, only two sequences of period-adding and simple period-adding, are rather simple while theirs are complicated in such a way that the state sequence can be described not only by the Farey tree but also by the Farey triangle, and (3) our state transition could be modelled by eq.(4) with z of either 2 or 3, but theirs is

uncertain. Therefore, we could say that our squid axon system is simpler as the frequency locking takes place on a two-torus system than theirs involving a three-or-more torus system. It should be noted here that the bifurcation to chaos in Region II could be also understood by application of the circle-map theory of Jensen, Bak and Bohr³⁷ to the restricted region of the macroscopic two-dimensional bifurcation structure; that is, our quasi-periodic response obtained for T of 2.6 msec (Fig.9), our phase-locked one obtained for T of 2.8 msec (Fig.10) and our chaotic one obtained for T of 3.0 msec (see Fig.6) may correspond to their phase-locked plus quasi-periodic responses for $k < 1$, their phase-locked response for $k = 1$ and their chaotic one for $k > 1$, respectively. However, the circle map description is only applicable to a restricted region of the two-dimensional bifurcation diagram (Fig.6) since only specific sequences have been observed in the global diagram, as seen above.

The presence of chaos in Regions III and IV is another characteristic. This may be qualitatively understood similarly to the case of self-oscillatory systems exposed to periodic input^{7,11,38-44}, as follows; periodic inputs have double effects on the axon at rest. One of the effects is, of course, that they exert as a periodic external force. The other is that they induce the axon to behave as self-oscillatory system. For the experimental evidence supporting the latter, we recently found that the repetitive firing of action potentials could be stably evoked in the isolated squid giant axon bathed in NSW by externally applied and outwardly-directed step current (Hanyu and Matsumoto, in preparation). The repetitive firing frequency was dependent on both the current intensity and temperature; the higher the current intensity (or temperature) was, then the higher the frequency became. These show that the oscillatory character inherently retained in normal axons could be amplified even by external steady current. Therefore, chaotic responses in the squid axon at rest could be evoked through a specific non-linear interaction between externally applied periodic

input and its induced oscillation. The fact that phase-locked responses were only concentrated in particular regions (Regions I and II) in the bifurcation diagram (Fig.6) could be qualitatively understood in this way; in these regions, the input, as it is regarded as strong stimulation, could suppress the oscillation inherent to the axon. Furthermore, the reason why the quenching (or the 0 response) appeared in a weakly stimulated region of the diagram (Fig.6) could be also explained in a similar way.

Quantitative analysis for the two-dimensional bifurcation diagram is left for future studies, although a preliminary study has been tried⁴⁵. For these analyses, the above qualitative considerations should definitely be of some help. So far, the theoretical studies have mainly focused on the analysis of response characteristic of self-oscillatory nerve membranes to periodic input. The response characteristic was studied for the Hodgkin-Huxley (H-H) model^{11,46,47}, the Fitzhugh-Nagumo model⁴⁸, the Caianiello model^{27-29,49} and various integrate-and-fire models⁵⁰⁻⁵². Like others, we have extensively studied the characteristics of spontaneously fired axons of squid and quantitatively compared these experiments with those of self-oscillatory H-H axons under periodic input^{11,12}. In both axons, we found three responses; phase-locked, quasi-periodic and chaotic. These are exactly the same responses as found in the present experiment. Furthermore, we found three routes to chaos in the H-H axon; (1) successive period-doubling⁵³, (2) intermittency^{23,34,35} and (3) collapse of quasi-periodicity^{54,55}, among which the former two bifurcations, (1) and (2), were experimentally observed in spontaneously fired squid giant axons^{8,11,12}. These similarities between the response patterns and the bifurcation routes found in normal axons and those found in self-sustaining ones could be ascribed to the reasons described in the above paragraph. The simulation experiments to obtain the bifurcation structure of the potential response pattern as a function

of I/I_t and T are now being studied for normal H-H axons when stimulated by a train of periodic current pulses.

Acknowledgements

We would like to express our sincere thanks to Professor Hisanao Ogura, Kyoto University, for his helpful advice, comments and support. We are particularly grateful to Professors Jin-ichi Nagumo and Shuji Yoshizawa, Tokyo University, and also to Dr. Kazuyuki Aihara, Tokyo Denki University, for their collaboration at the initial stage of the present work.

Figure Captions

Fig.1 : Schematic diagram of experimental setup. A chamber, temperature-controlled within $\pm 0.01^\circ\text{C}$ in the temperature range 4 through 18°C and with a width of 51 mm, is filled with natural seawater (NSW). A squid giant axon (AXON) is bathed in NSW. Stimulating current pulse (STIMULATION) is given to an internal electrode (S) of platinized-platinum of 5 mm in length through a resistor of $470\text{ k}\Omega$ by a pulse generator. Nonpropagating potential responses are monitored with a pair of glass-pipette electrodes of the Ag-AgCl type, internal (R_2) and external (R_1) ones, through an amplifier of high input impedance (V_1). Propagating responses are also measured with a pair of glass-pipettes electrodes of Ag-AgCl type, R_1 and R_3 , through an amplifier of high input impedance (V_2). The internal electrode R_3 is placed about 30 mm away from the other electrode R_2 . G : a Ag-AgCl coil to ground NSW.

Fig.2 : Propagating (Record 1) and nonpropagating (Record 2) potential responses of the squid giant axon to a train of periodic current pulses (Record 3) where the current intensity normalized by the current threshold, I/I_t , is kept constant at 1.5 and time intervals between neighbouring current pulses, T , are changed: A; $T = 6.4\text{ msec}$. B; $T = 6.2\text{ msec}$. C; 5.6 msec . Temperature; 14.0°C .

Fig.3 : Latency (τ_n) as a function of sequence number (n) at which the action potential is evoked. *Upper* : Schematic drawing to illustrate how τ_n is defined in a relation between nonpropagating action potentials (upper trace) and current pulses (lower trace). *Lower* : A; the τ_n vs. n relation for the potential pattern 1 corresponding to Record 2 in Fig.2A. B; the τ_n vs. n relation for the potential pattern 190 corresponding to Record 2 in

Fig.2B. C; the τ_n vs. n relation for the potential pattern 1²⁰ corresponding to Record 2 in Fig.2C.

Fig.4 : (1) The τ_{n+2} vs. τ_n plot for the potential pattern 1²⁰ corresponding to Record 2 in Fig.2C. (2) Normalized MEM spectrum as a function of frequency for the potential pattern 1²⁰ corresponding to Record 2 in Fig.2C. The frequency spectrum was calculated by the maximum entropy method (MEM).

Fig.5 : Time intervals, t_n , between neighbouring action potentials as a function of sequence number, n , of the action potential. *Upper* : Schematic drawing to illustrate how t_n is defined in a train of action potentials (upper trace) evoked by periodic current pulses (lower trace). *Lower* : A; the t_n vs. n relation for the potential pattern 1 the t_n vs. n relation for the potential pattern 1⁹⁰ corresponding to Record 2 in Fig.2B. C; the t_n vs. n relation for the potential pattern 1²⁰ corresponding to Record 2 in Fig.2C.

Fig.6 : A global bifurcation diagram of potential response patterns as a function of the current intensity normalized by the current threshold (I/I_t) and time intervals, T , between neighbouring current pulses (Pulse Interval). See details in the text.

Fig.7 : (A) Firing rates as a function of I/I_t for the 1ⁿ⁰ responses where $n = 1, 2, 3, \dots, \infty$. T (time intervals between neighbouring current pulses) is kept constant at 5.0 msec. (B) τ_n vs. n relations for the 1ⁿ⁰ responses, obtained when $T = 5.0$ msec, where $I/I_t = 1.43$ (a), 1.75 (b), 1.76 (c), 1.86 (d), 1.87 (e) and 1.96 (f), respectively. The values of I/I_t at which the respective τ_n vs. n relations (a, b, c, d, e and f), are obtained correspond to those shown above as a, b, c, d, e and f, respectively.

Fig.8 : (A) Firing rates as a function of I/I_t for the 1ⁿ⁰ responses obtained when $T = 6.0$ msec. (B) τ_n vs. n relations for the responses obtained when $T = 6.0$ msec and $I/I_t = 1.620$ (a), 1.625 (b), 1.630 (c), 1.646 (d), 1.688 (e) and

1.719 (f), respectively. Firing rates obtained for these values of I/I_t are shown above as a, b, c, d, e and f, respectively.

Fig.9 : (A) Firing rates as a function of I/I_t for the $(10)^{n-1}100$ responses obtained when $T = 2.6$ msec. (B) τ_n vs. n relations for the responses obtained when $T = 2.6$ msec and $I/I_t = 1.80$ (a), 1.83 (b), 1.87 (c), 1.90 (d), 1.93 (e) and 1.97 (f), respectively. Firing rates for these values of I/I_t are shown above as a, b, c, d, e and f, respectively.

Fig.10 : (A) Firing rates as a function of I/I_t for the $(10)^{n-1}100$ responses obtained when $T = 2.8$ msec. (B) τ_n vs. n relations for the responses obtained when $T = 2.8$ msec and $I/I_t = 1.40$ (a), 1.66 (b), 1.69 (c), 1.75 (d), 1.76 (e) and 1.79 (f), respectively.

Fig.11 : Normalized MEM spectrum as a function of frequencies. The spectral density was calculated with the maximum entropy method (MEM). (A) The power spectral densities calculated from the data of the $(10)^{n-1}100$ firing responses obtained when $T = 2.6$ msec and $I/I_t = 1.83$ (b), 1.87 (c) and 1.90 (d), respectively. The same data was used as those for Fig.9. (B) The power spectral densities calculated from the data of the $(10)^{n-1}100$ firing responses obtained when $T = 2.8$ msec and $I/I_t = 1.69$ (c), 1.75 (d) and 1.76 (e), respectively.

Fig.12 : Firing rates as a function of I/I_t for the potential responses obtained when $T = 3.8$ msec. The firing rates designated as a through o are characterized as the relations of t_n vs. n , a through o in Fig.13, respectively.

Fig.13 : Relations of t_n vs. n for the potential response obtained when $T = 3.8$ msec. The relations a through o are calculated from the data of the responses obtained when $I/I_t = 1.102$ (a), 1.142 (b), 1.148 (c), 1.165 (d), 1.193 (e), 1.199 (f), 1.210 (g), 1.215 (h), 1.233 (i), 1.239 (j), 1.256 (k), 1.273 (l), 1.284 (m), 1.307 (n) and 1.335 (o), respectively.

Fig.14 : (A) Firing rates as a function of I/I_t for the potential responses obtained when $T = 4.0$ msec. (B) The relations of t_n vs. n for the potential responses obtained when $T = 4.0$ msec and when $I/I_t = 1.212$ (a), 1.228 (b), 1.239 (c), 1.252 (d), 1.271 (e) and 1.278 (f), respectively.

Fig.15 : Relations of $\{(I/I_t)_\infty - (I/I_t)_n\}$ vs. n for the 1^{n0} potential responses obtained when $T = 5.0$ msec (o), 6.0 msec (Δ) and 6.5 msec (*), respectively, where I/I_∞ and $(I/I_t)_n$ are defined as the minimum values of I/I_t above which the 1 and $1^{n+1}0$ responses appear, respectively. The relations are best-fitted with lines of $n^{-\lambda}$ where $\lambda = 1.8 \pm 0.1$, -2.0 ± 0.2 and -2.0 ± 0.3 for the data obtained when $T = 5.0$ msec, 6.0 msec and 6.5 msec, respectively.

Fig.16 : Relations of $\{(I/I_t)_\infty - (I/I_t)_n\}$ vs. n for the $(10)^{n-1}100$ potential responses obtained when $T = 2.6$ msec (o) and 2.8 msec (Δ), respectively, where $(I/I_t)_\infty$ and $(I/I_t)_n$ are defined as the minimum values of I/I_t above which the 10 and $(10)^{n-1}100$ responses appear. The relations are best-fitted with lines of $n^{-\lambda}$ where $\lambda = 1.2 \pm 0.1$ and 1.3 ± 0.3 and for the data obtained when $T = 2.6$ msec and 2.8 msec respectively.

Fig.17 : Numbers of a Farrey's series to the 12th order. the numbers of $n/(n+1)$ (i.e., $\frac{1}{2}, \frac{2}{3}, \frac{3}{4}, \dots, \frac{11}{12}$), $n/(2n+1)$ (i.e., $\frac{1}{3}, \frac{2}{5}, \dots, \frac{5}{11}$), 1 and 0 corresponds to firing rates for the phase-locked or quasi-periodic responses of 1^{n0} , $(10)^{n-1}100$, 1 and 0 in Fig.6. The chaotic responses are observed between both 0/1 and 1/2 (hatched region) and between $n/(2n+1)$ and $(n+1)/(2n+3)$ (dotted regions) where $n = 1, 2, 3$ and 4 (see also Fig.6).

References

1. A.P.Fein, M.S.Heutmacher and J.P.Gollub, Phys.Scr. T9, 79(1985).
2. J.Stavans, F.Heslot and A.Libchaber, Phys.Rev.Lett. 55, 596(1985).
3. J.Martin and W.Martienssen, Phys.Rev.Lett. 56, 1522(1986).
4. S.E.Brown, G.Mozurkewein and G.Gruner, Phys.Rev.Lett. 52, 2277(1984).
5. J.Maselko and H.L.Swinney, Phys.Scr. T9, 35(1985).
6. J.Maselko and H.L.Swinney, J.Chem. Phys. 85, 6430(1986).
7. M.R.Guevara, L.Glass and A.Shrier, Science 214, 1350(1980).
8. G.Matsumoto, K.Aihara, M.Ichikawa and A.Tasaki, J.theor.Neurobiol. 3, 1(1984).
9. P.Bak, Physics Today 39-12, 38(1986).
10. G.Matsumoto, Long-Range Spatial Interactions and a Dissipative Structure in Squid Giant Axons and a Proposed Physical Model of Nerve Excitation, in "Nerve Membrane, Biochemistry and Function of Channel Proteins", ed. by G.Matsumoto and M.Kotani (The Univ. of Tokyo Press, Tokyo, 1981) p.203.
11. K.Aihara and G.Matsumoto, Chaotic Oscillations and Bifurcations in Squid Giant Axons, in "Chaos", ed. by A.V.Holden (Manchester Univ. Press, Princeton, N.J., 1986) p.257.
12. K.Aihara and G.Matsumoto, Forced Oscillations and Routes to Chaos in the Hodgkin-Huxley Axons and Squid Giant Axons, in "Chaos in Biological Systems", ed by H.Degn, A.V.Holden and L.F.Olsen (Plenum Pub.Corp., 1987) p.121.
13. G.Matsumoto, N.Takahashi and Y.Hanyu, Chaos, Phase Locking and Bifurcation in Normal Squid Axons, in "Chaos in Biological Systems", ed. by H.Degn, A.V.Holden and L.F.Olsen (Plenum Pub.Corp., 1987) p.143.

14. G.Matsumoto, K.Aihara, Y.Hanyu, N.Takahashi, S.Yoshizawa and J.Nagumo, *Phys.Lett.A* 123, 162(1987).
15. G.Matsumoto, *Biol.Bull.* 150, 279(1976).
16. G.Matsumoto and J.Shimada, *Biol.Bull.* 159, 319(1980).
17. M.Ichikawa and G.Matsumoto, to be submitted to *J. Neuroscience*.
18. I.Tasaki, *Nerve Excitation, A Macromolecular Approach* (Charles C.Thomas Pub., Springfield, Mass., 1968).
19. A.L.Hodgkin, *The Conduction of the Nervous Impulse* (Liverpool Univ.Press, Liverpool, 1964).
20. A.L.Hodgkin and A.F.Huxley, *J.Physiol. (London)* 117, 500(1952).
21. L.D.Harmon, *Kybernetik* 1, 89(1961).
22. J.P.Burg, *Maximum Entropy Spectral Analysis*, A paper presented at the 37th Annual International Meeting for Society of Explor.Geophys. (Oklahoma City, Oklahoma, Oct. 31, 1967).
23. Y.Pomeau and P.Manneville, *Commun.Math.Phys.* 74, 189(1980).
24. P.Berge, Y.Pomeau and C.Vidal, "Order within Chaos-Towards a Deterministic Approach to Turbulence", translated from the French edition by L.Tukerman (John Wiley & Sons, New York, 1986).
25. J.M.T.Thompson and H.B.Stewart, "Nonlinear Dynamics and Chaos" (John Wiley & Sons, Chichester, 1986).
26. I.Tsuda, *Prog.Theor.Phys.* 66, 1985(1981).
27. J.Nagumo and S.Sato, *Kybernetik* 10, 155(1972).
28. S.Yoshizawa, H.Osada and J.Nagumo, *Biol.Cybern.* 45, 23(1982).
29. M.Yamaguchi and M.Hata, in "Lectures Notes in Biomathematics, Vol.45, Competition and Cooperation in Neural Nets", ed. by S.Amari and M.A.Arbib (Springer, Berlin, 1982) p.171.
30. K.Kaneko, *Prog.Theor.Phys.* 68, 669(1982).
31. K.Kaneko, *Prog.Theor.Phys.* 69, 403(1983).

32. L.Glass and R.Perez, Phys.Rev.Lett. 48, 1772(1982).
33. R.Perez and L.Glass, Phys.Lett. 90A, 441(1982).
34. J.E.Hirsch, B.A.Huberman and D.J.Scalapino, Phys.Rev. 25A, 519(1982).
35. J.E.Hirsch, M.Nauenberg and D.J.Scalapino, Phys.Lett. 87A, 391(1982).
36. M.Sano and Y.Sawada, Phys.Lett. 97A, 73(1983).
37. M.H.Jensen, P.Bak and T.Bohr, Phys.Rev. A30, 1960(1984).
38. D.H.Perkel, J.H.Schulman, T.H.Bullock, G.P.Moore and J.P.Segunndo, Science 145, 61(1964).
39. L.Glass and M.C.Mackey, J.Math.Bkol. 7, 339(1979).
40. L.Glass, C.Graves, G.A.Petrillo and M.C.Mackey, J.theor.Biol. 86, 455(1980).
41. J.Belair, J.Math.Biol. 24, 217(1986).
42. M.R.Guevara and L.Glass, J.Math.Biol. 14, 1(1982).
43. L.Glass, M.R.Guevara, A.Shrier and R.Perez, Physica 7D, 89(1983).
44. L.Glass, M.R.Guevara, J.Belair and A.Shrier, Phys.Rev. 29A, 1348(1984).
45. J.P.Keener, F.C.Hoppensteadt and J.Rinzel, SIAM J.appl.Math. 41, 503(1981).
46. A.V.Holden, Biol.Cybernetics 21, 1(1976).
47. I.Nemoto, S.Miyazaki, M.Saito and T.Utsunomiya, Biophys.J. 15, 469(1975).
48. J.Flaherty and F.Hoppensteadt, Stud.Appl.Math. 58, 5(1987).
49. E.R.Caianiello, J.theor.Biol. 1, 204(1961).
50. B.W.Knight, J.Gen.Phys. 59, 734(1972).
51. A.Rescigno, R.B.Stein, R.L.Purple and R.E.Poppele, Bull.Math.Biophys. 32, 337(1972).
52. C.Ascoli, M.Barbi, S.Chillemi and D.Petracchi, Biophys.J. 19, 219(1977).
53. M.J.Feigenbaum, J.Stat.Phys. 19 (1978), 25; 21 (1979)669.
54. K.Kaneko, in "Chaos and Statistical Methods", ed. by Y.Kuramoto (Springer Verlag, Berlin, 1984) p.83.
55. S.Ostlund, D.Rand, J.Sethna and E.Siggia, Physica 8D (1983)303.

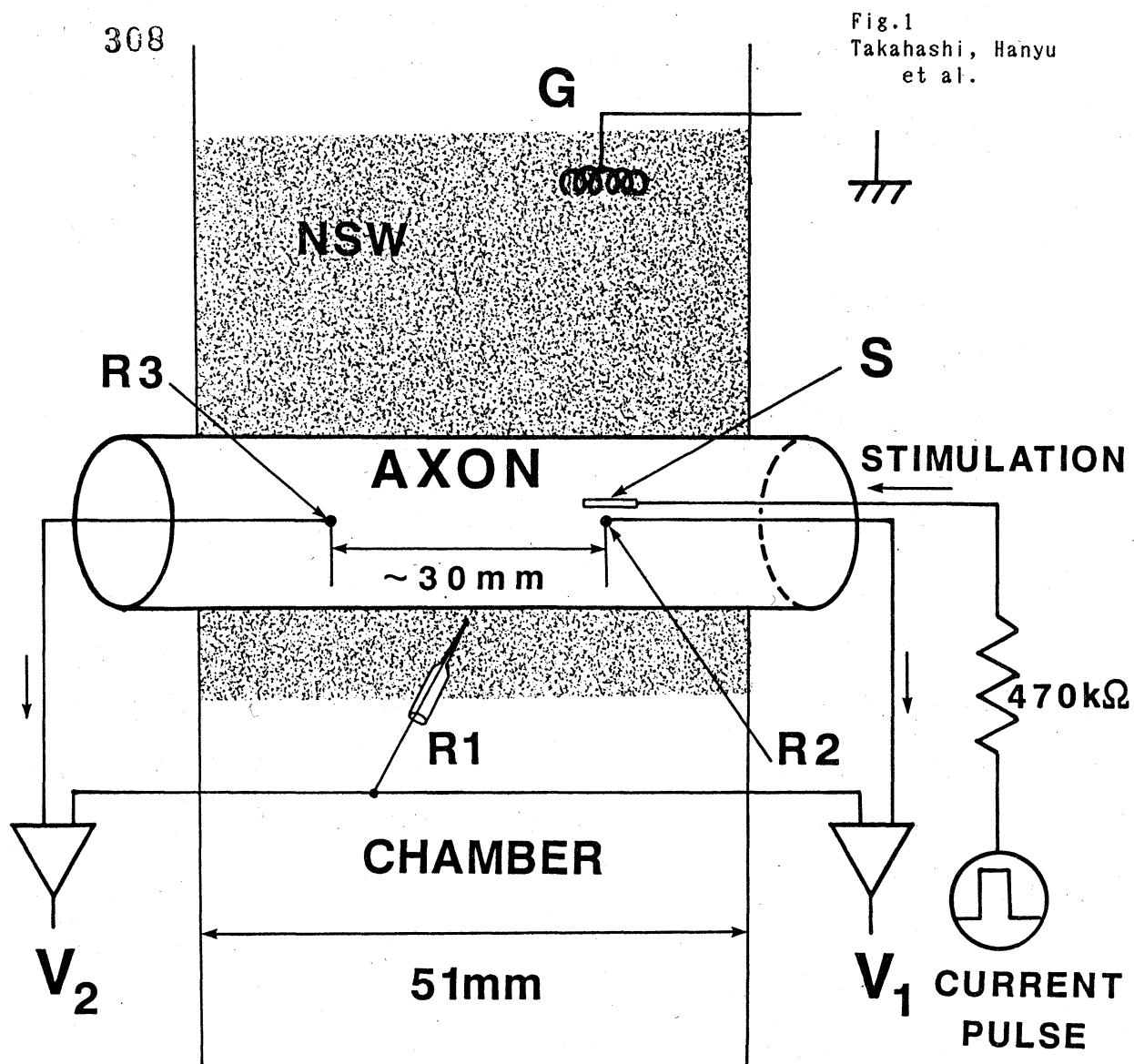


Fig.2
Takahashi, Hanyu
et al.

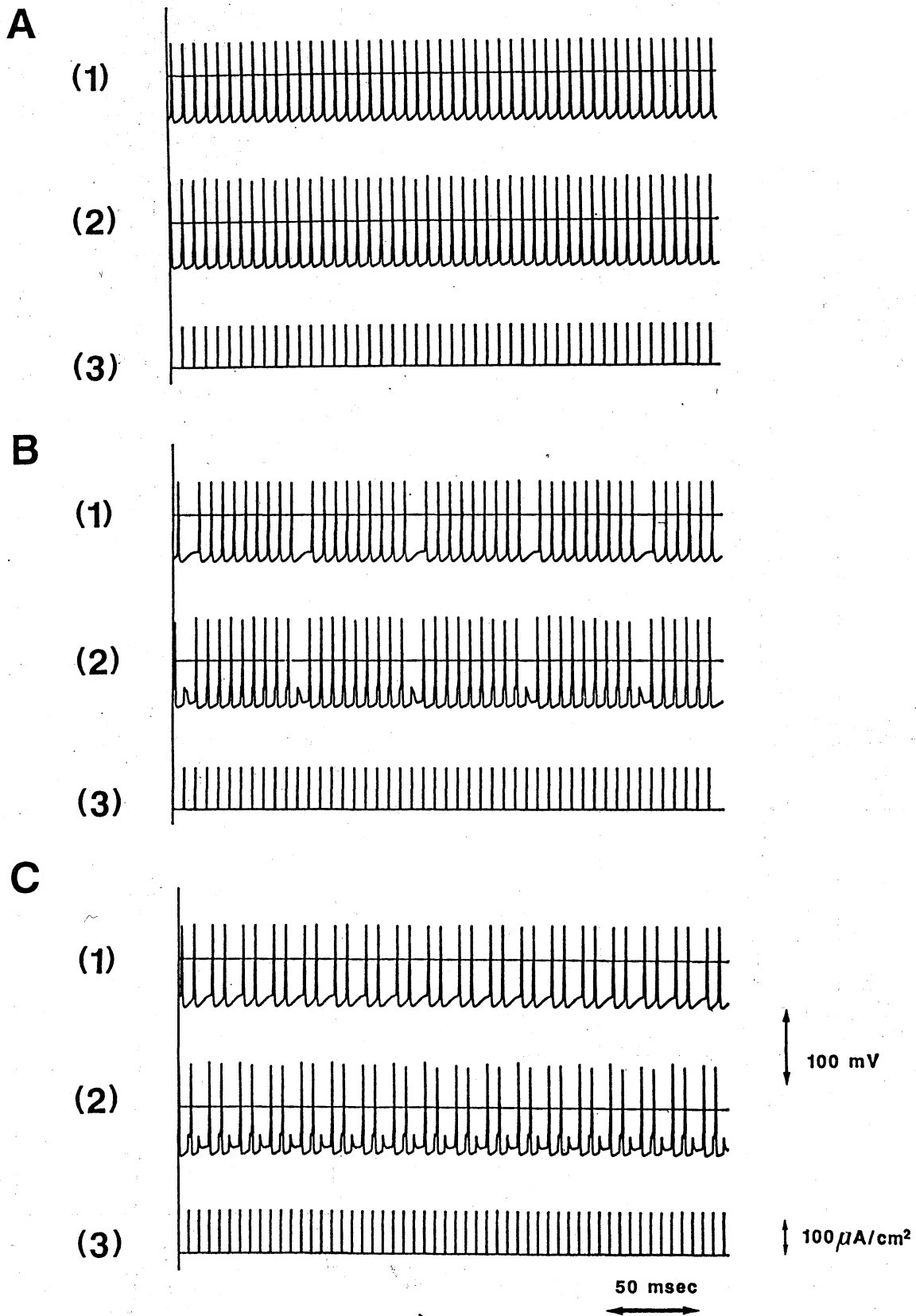
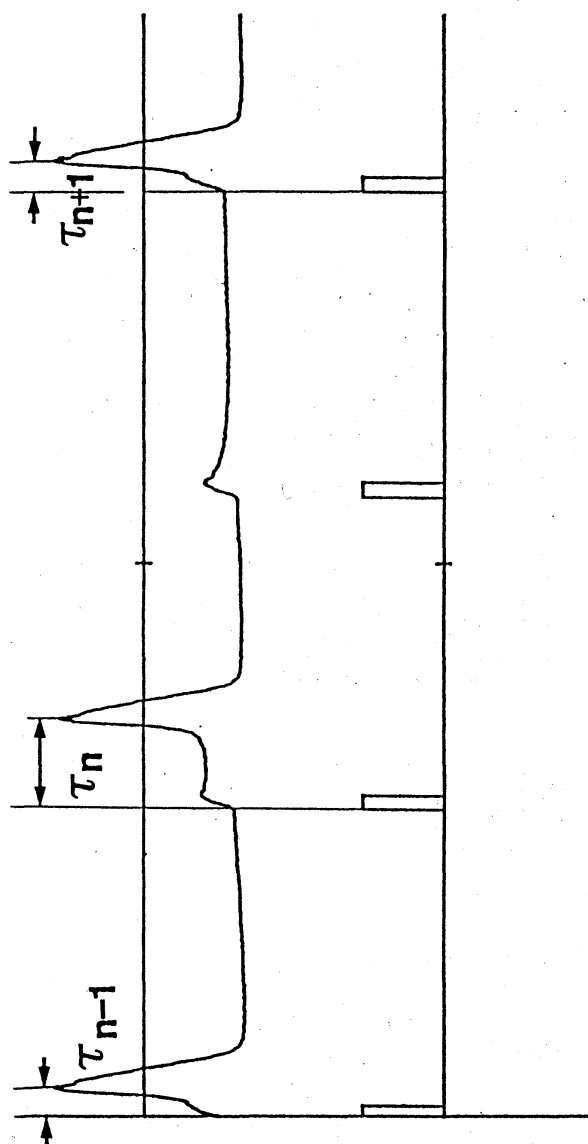
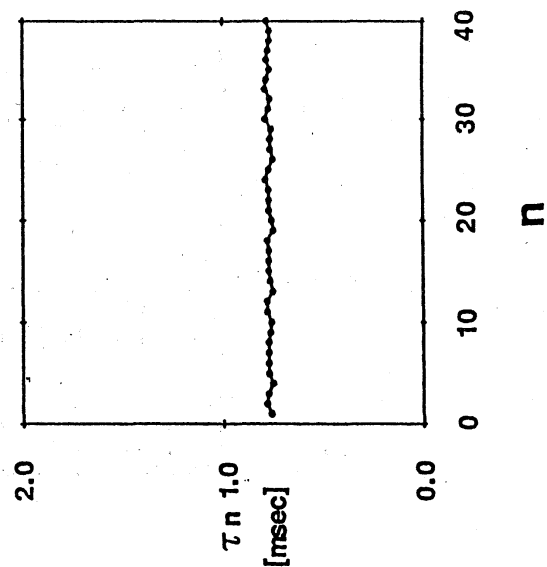


Fig.3
Takahashi, Hanyu
et al.

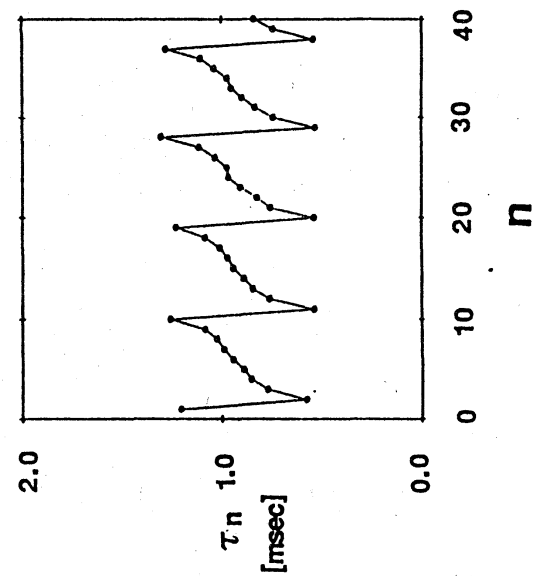


35

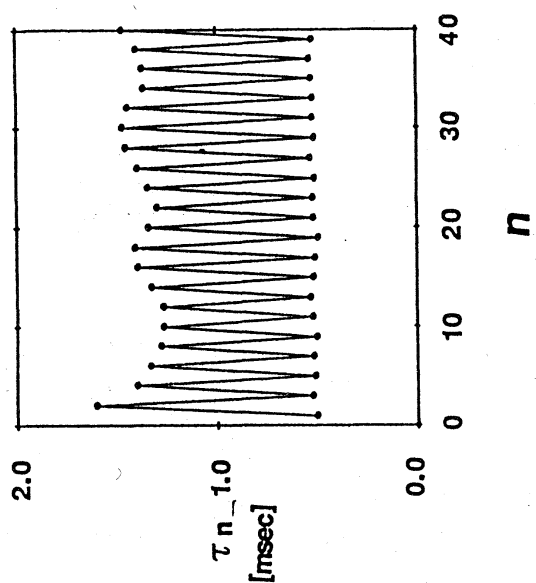
A



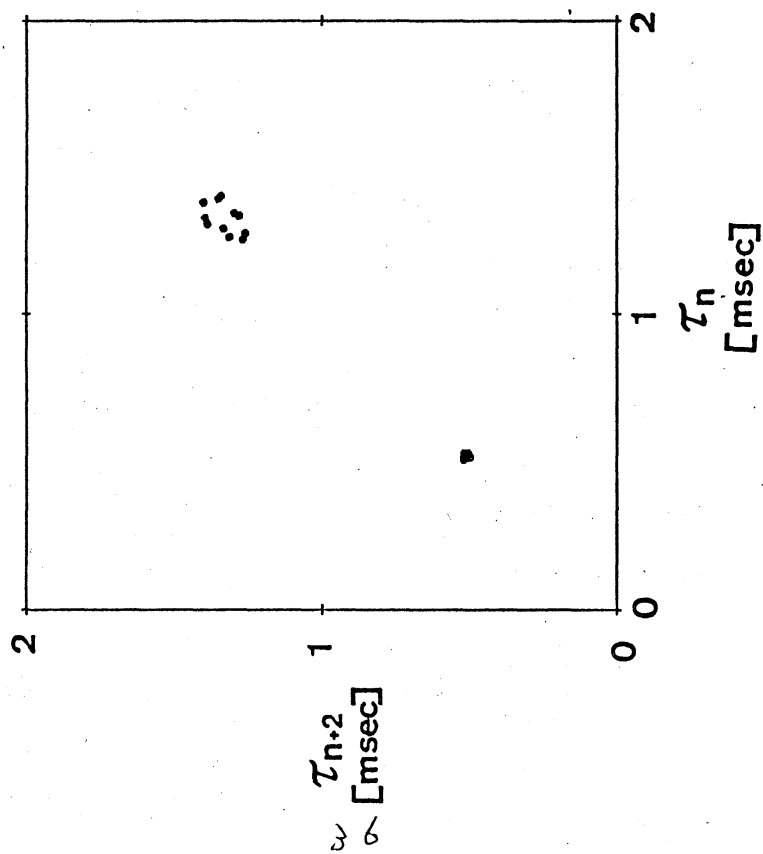
B



C



(1)



(2)

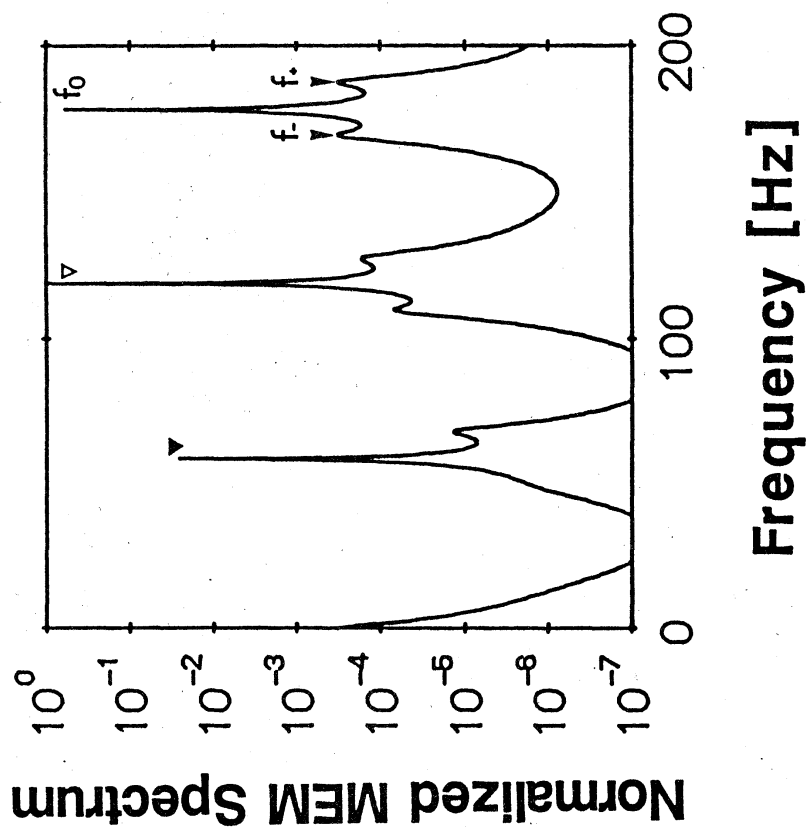
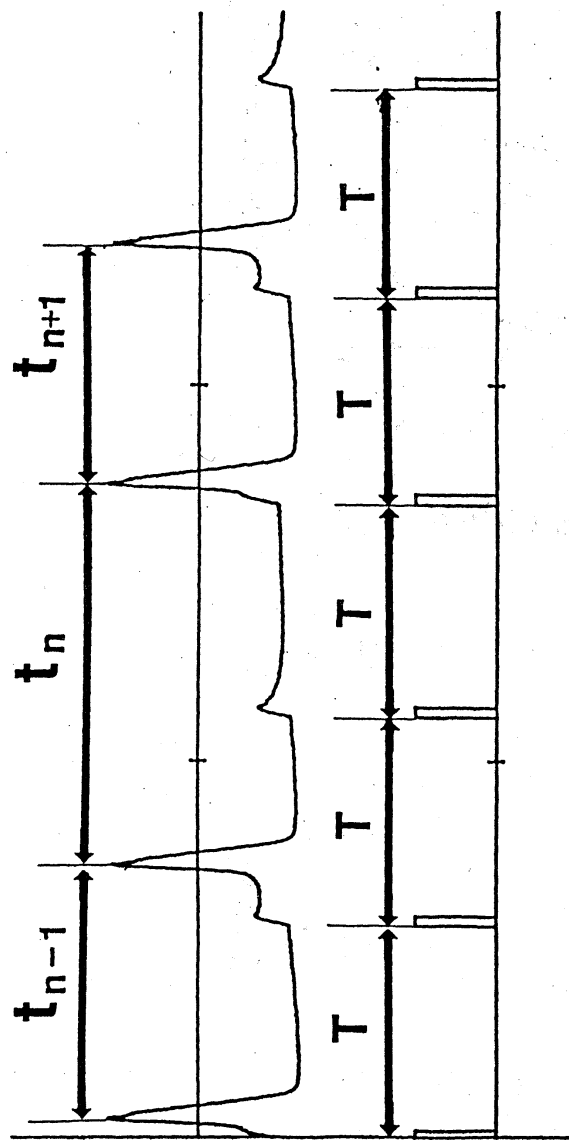


Fig.4
Takahashi, Hanyu
et al.



A

B

C

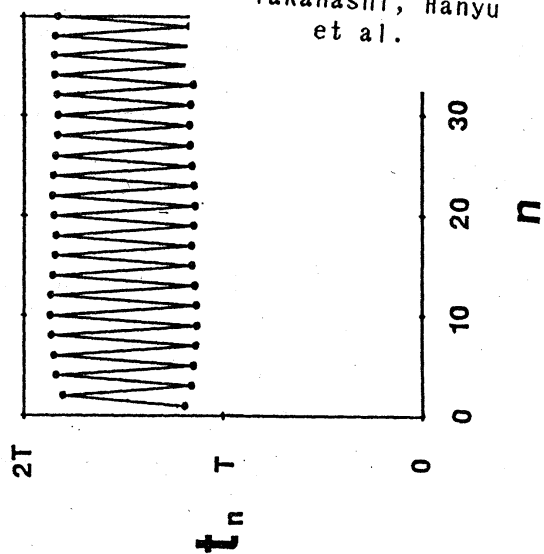
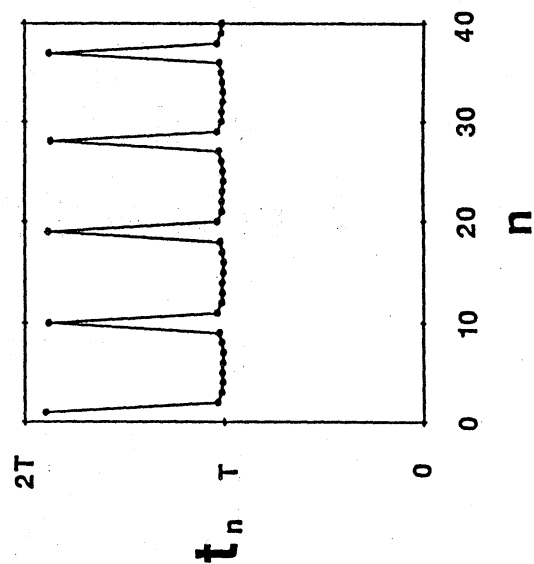
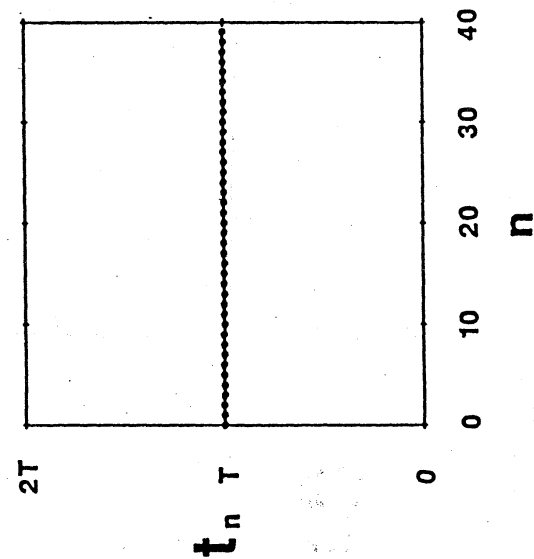
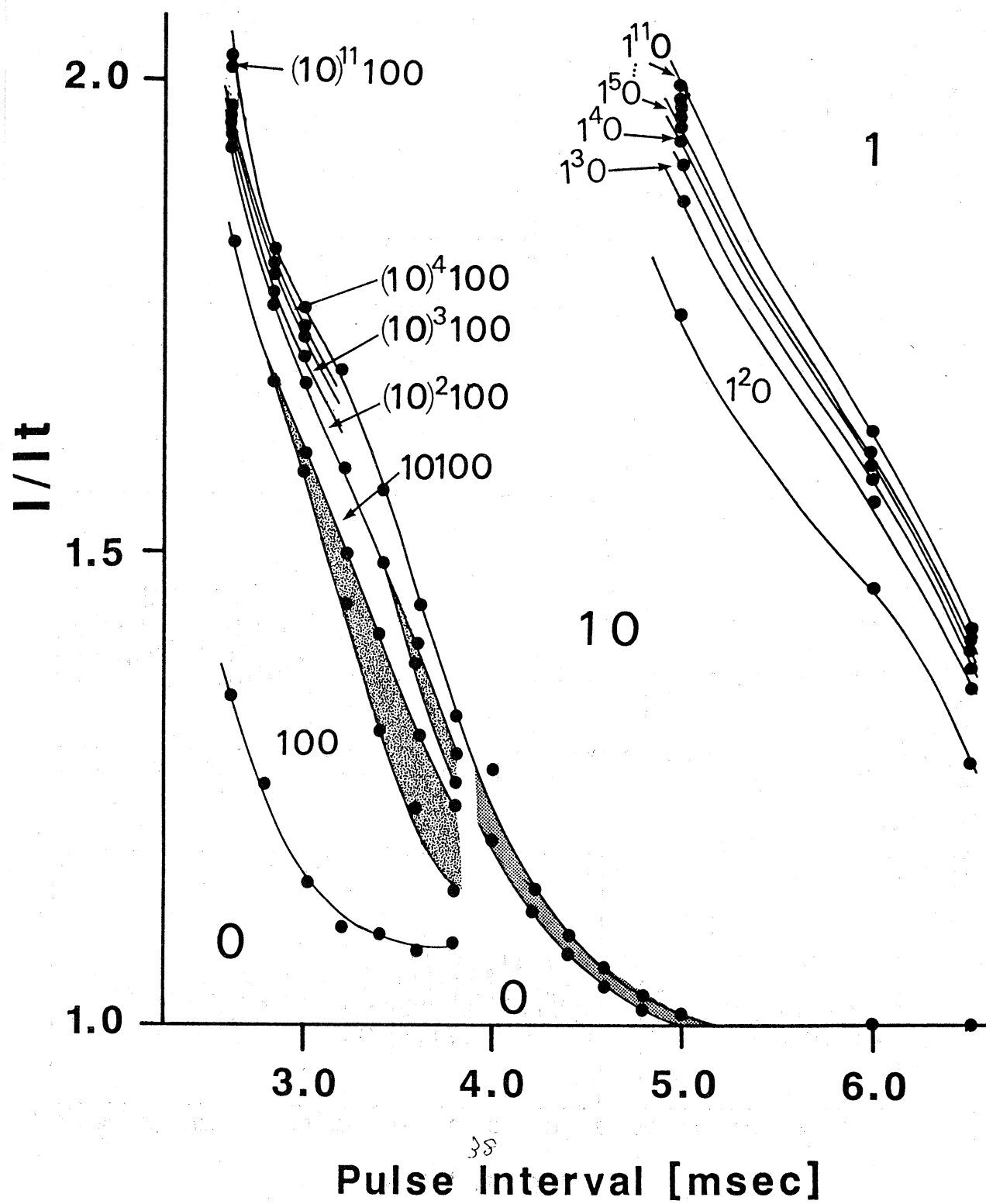
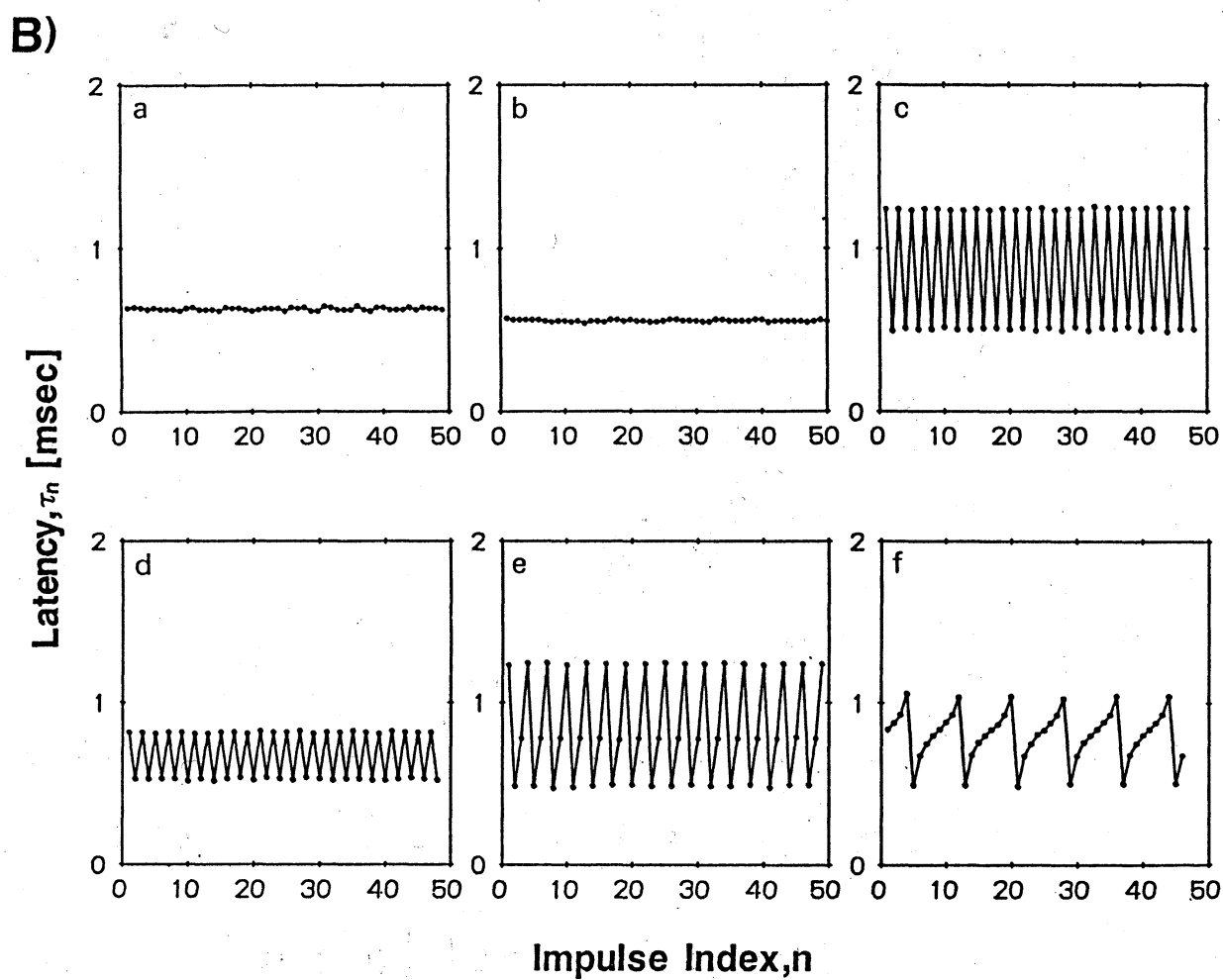
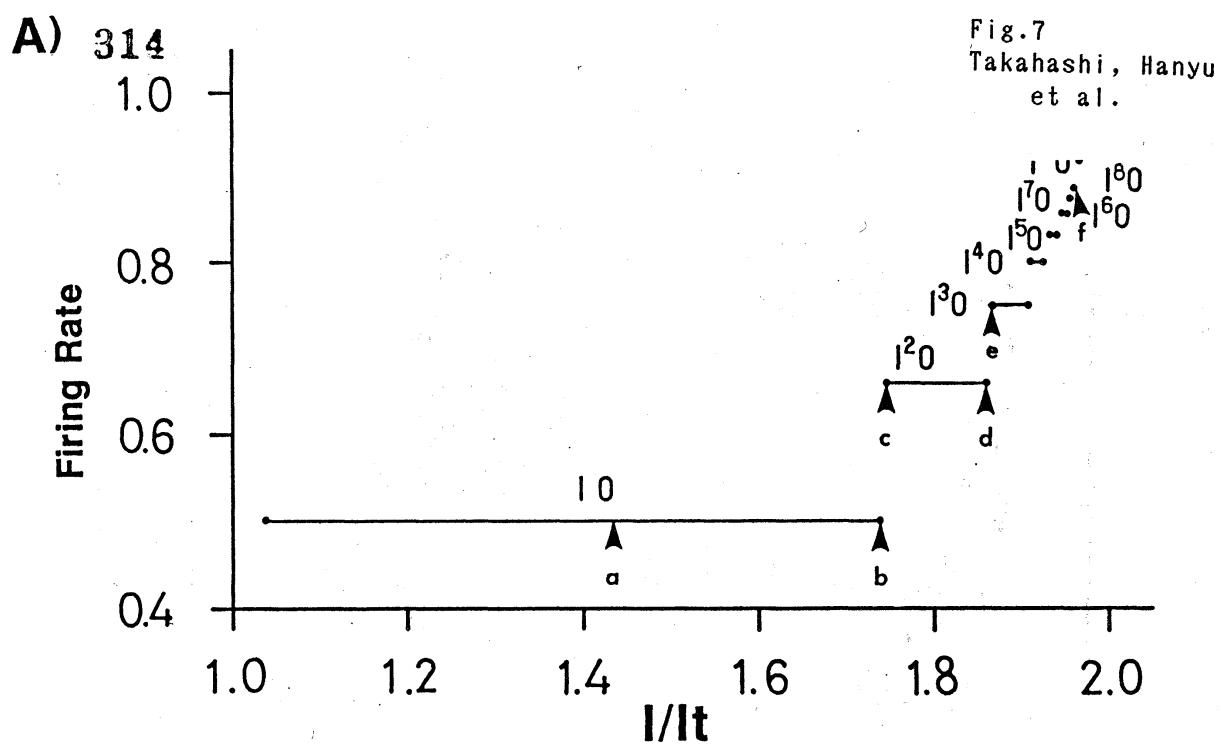


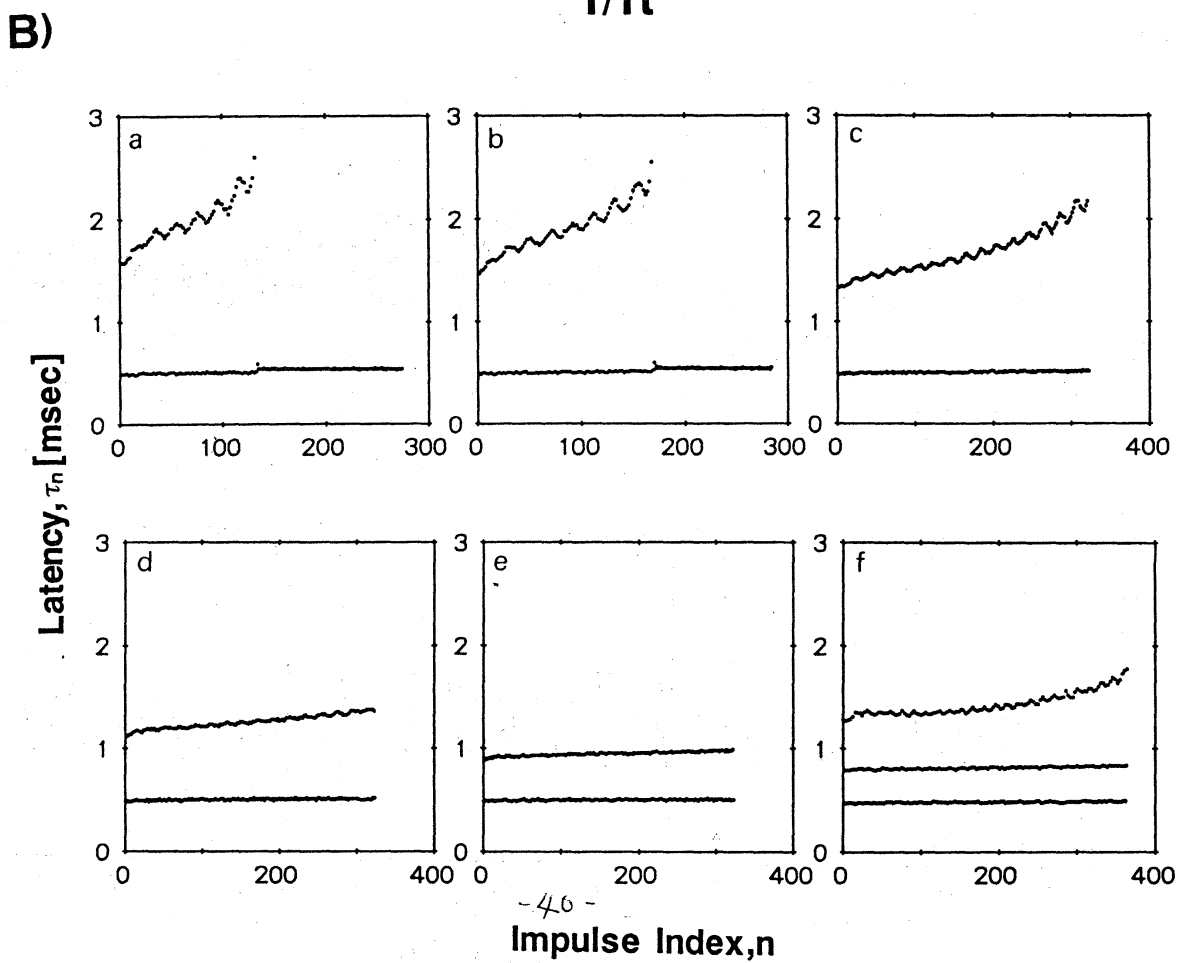
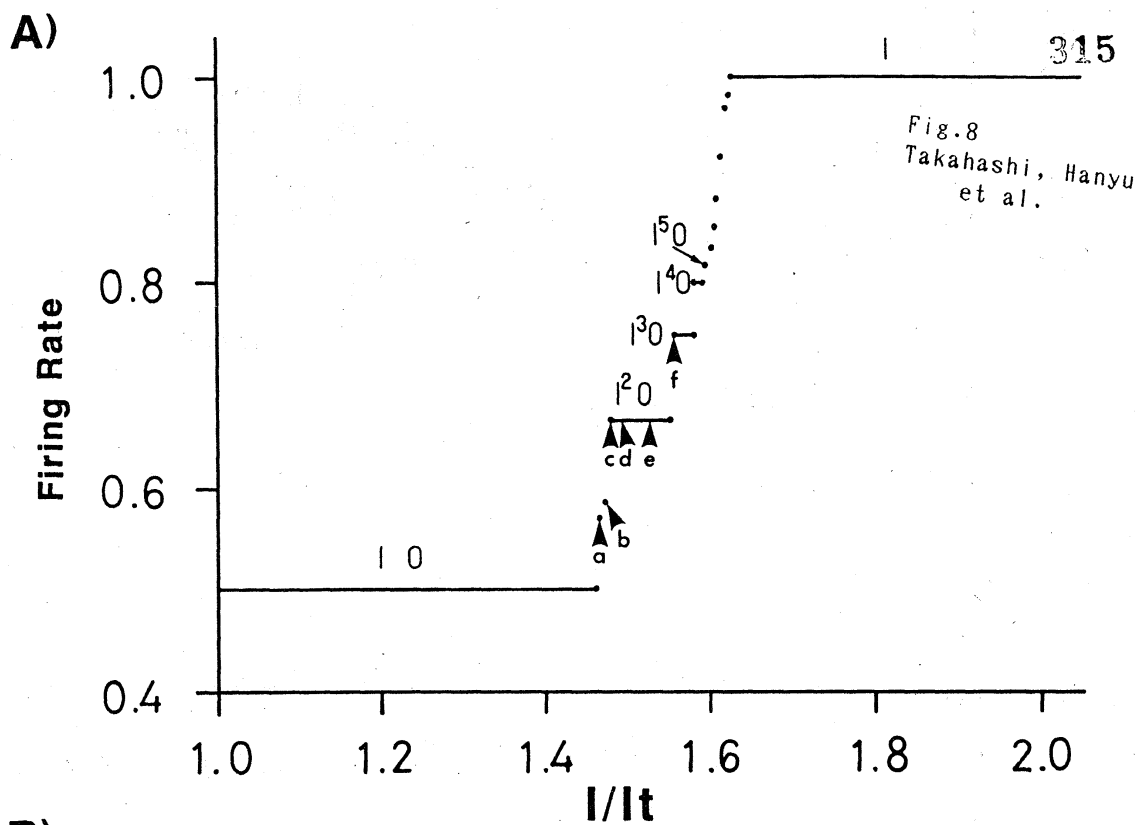
Fig.5
Takahashi, Hanyu
et al.

Fig.6
Takahashi, Hanyu
et al.

313







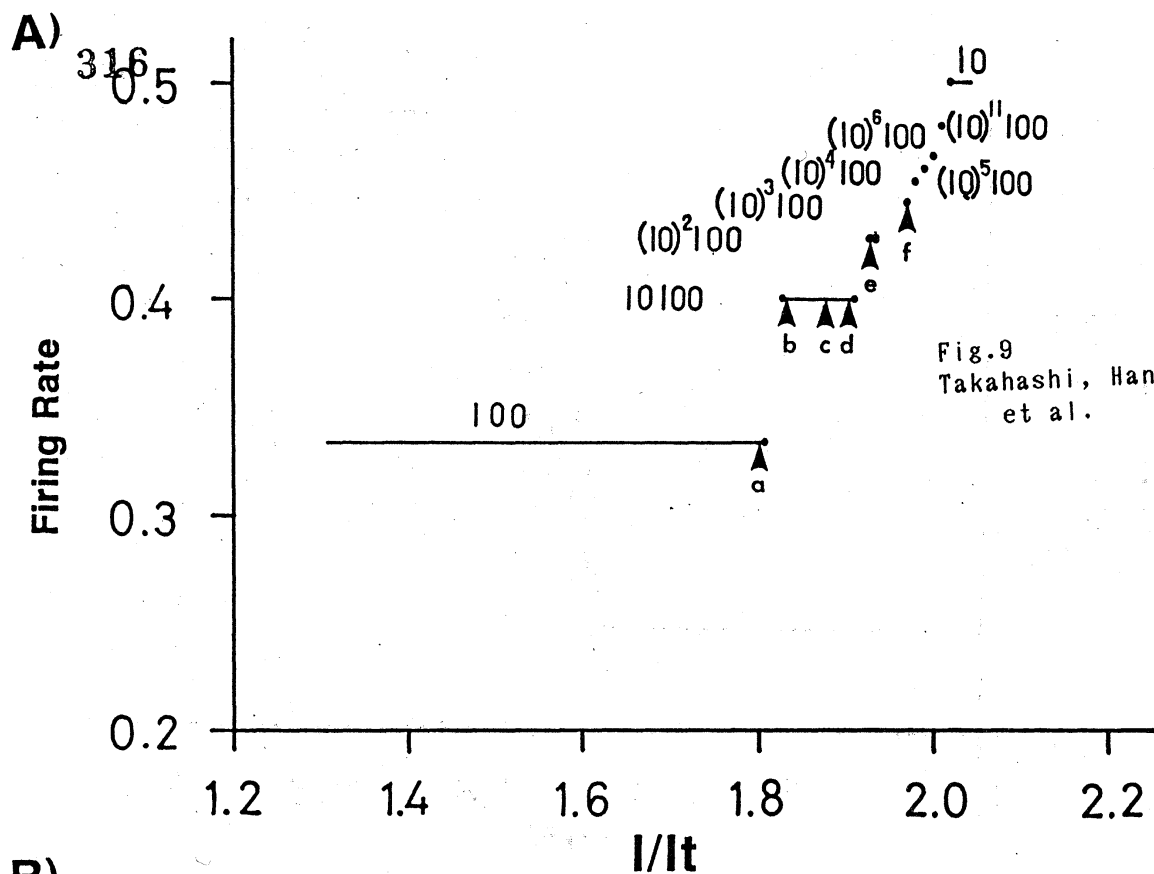
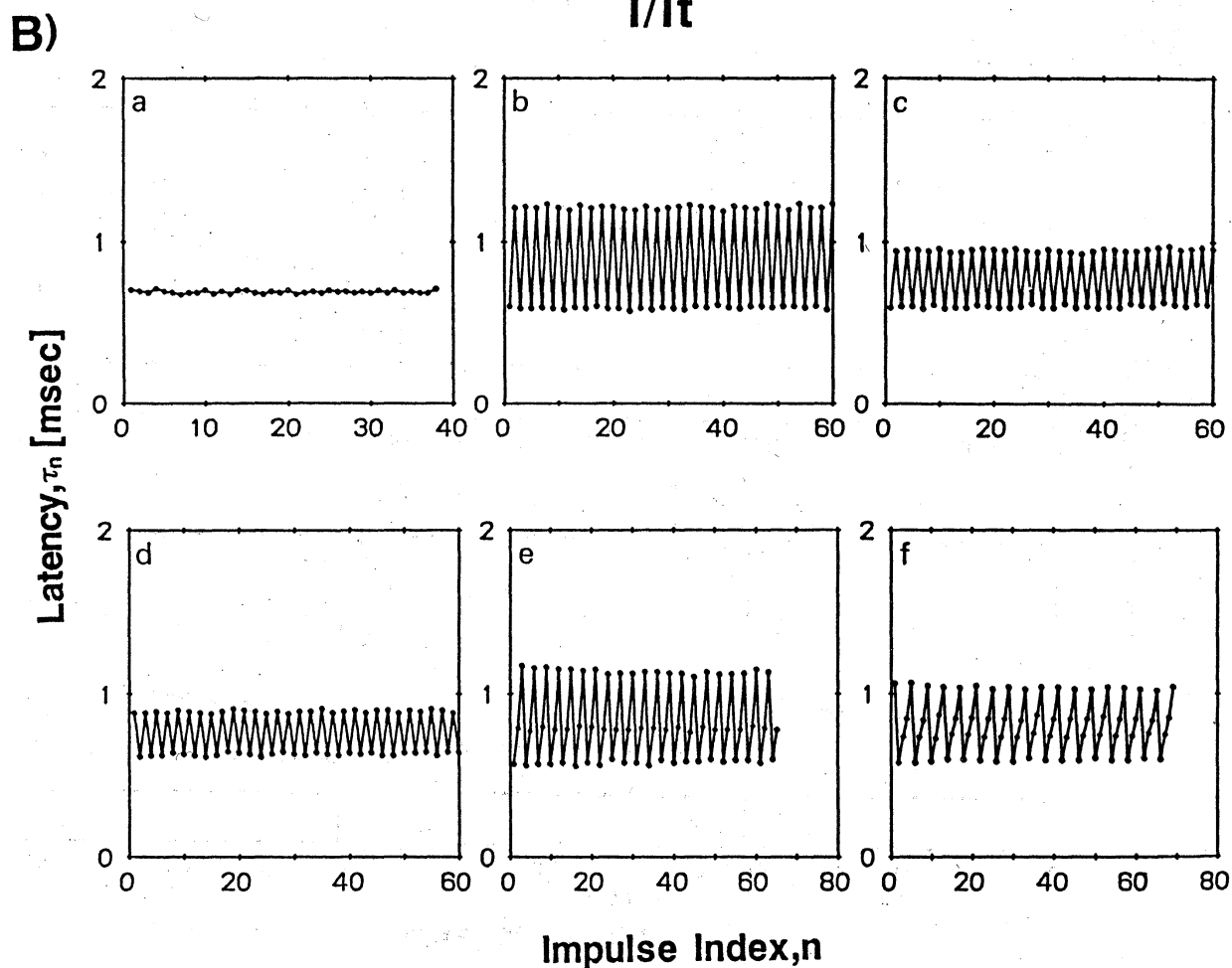


Fig.9
Takahashi, Hanyu
et al.



A)

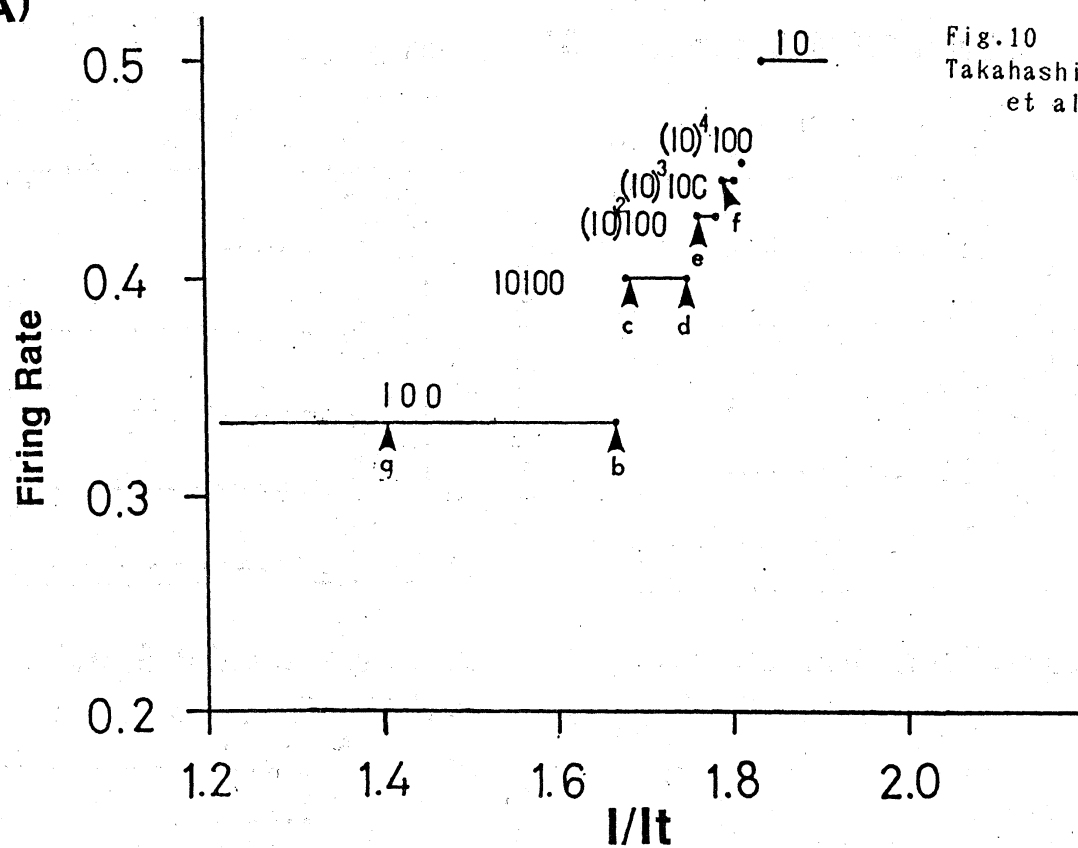
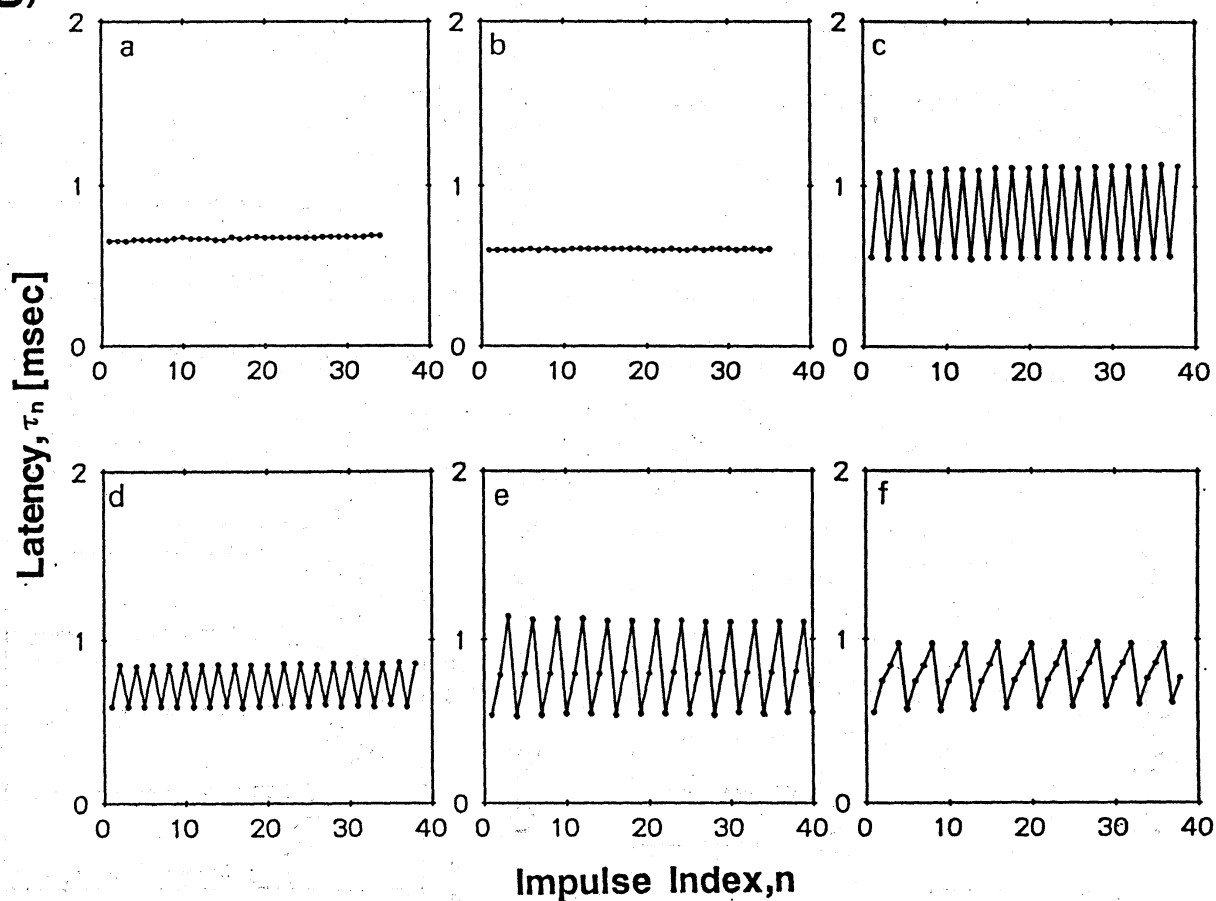


Fig.10
Takahashi, Hanyu
et al.

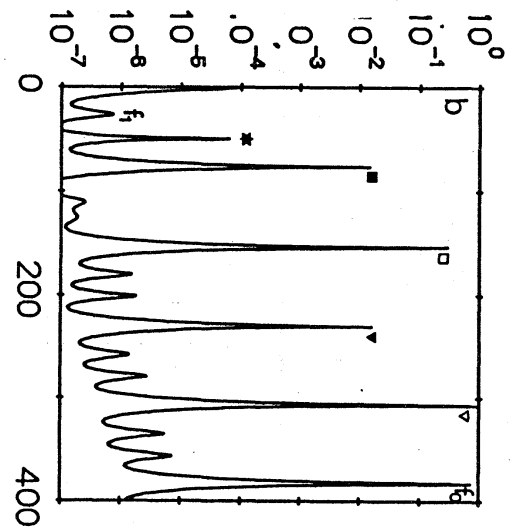
317

B)

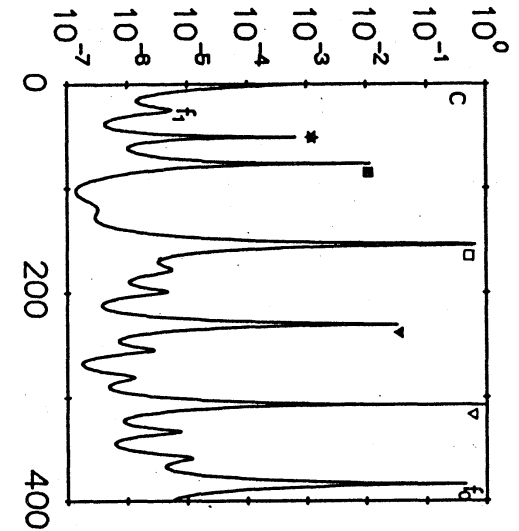


B

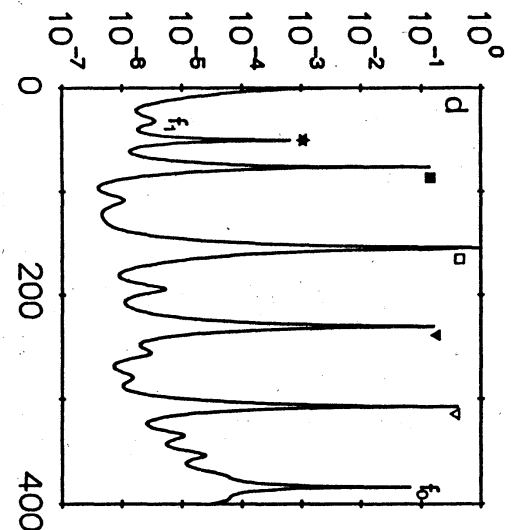
Normalized I



Normalized MEM Spectrum



Normalized MEM Spectrum

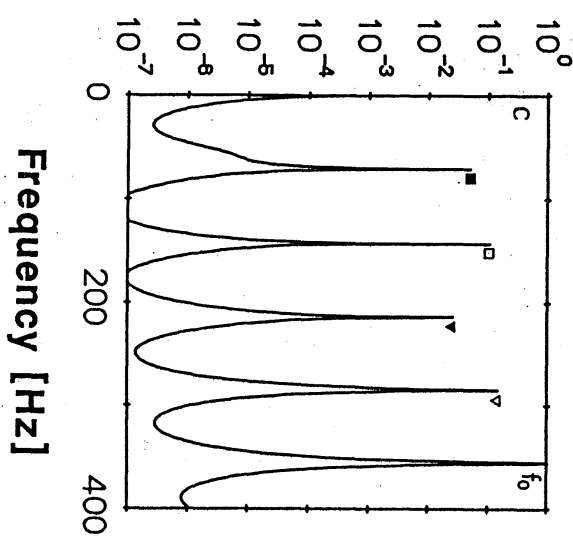


Frequency [Hz]

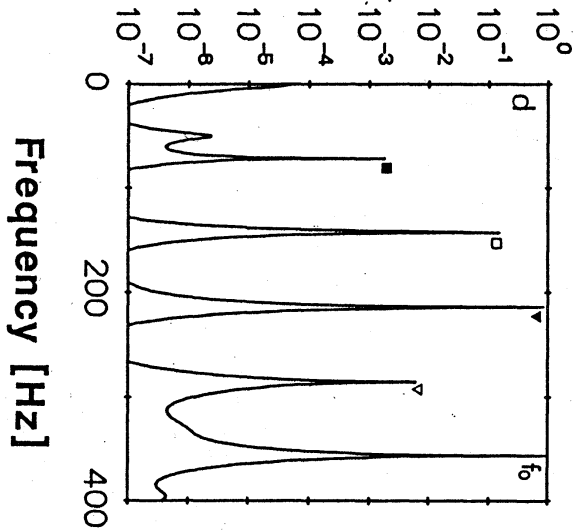
Frequency [Hz]

Frequency [Hz]

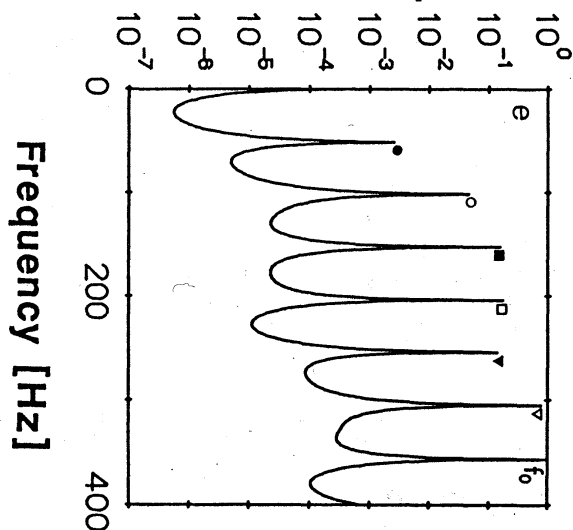
Normalized MEM Spectrum



Normalized MEM Spectrum



Normalized MEM Spectrum



Frequency [Hz]

Frequency [Hz]

Frequency [Hz]

Fig.12
Takahashi, Hanyu
et al.

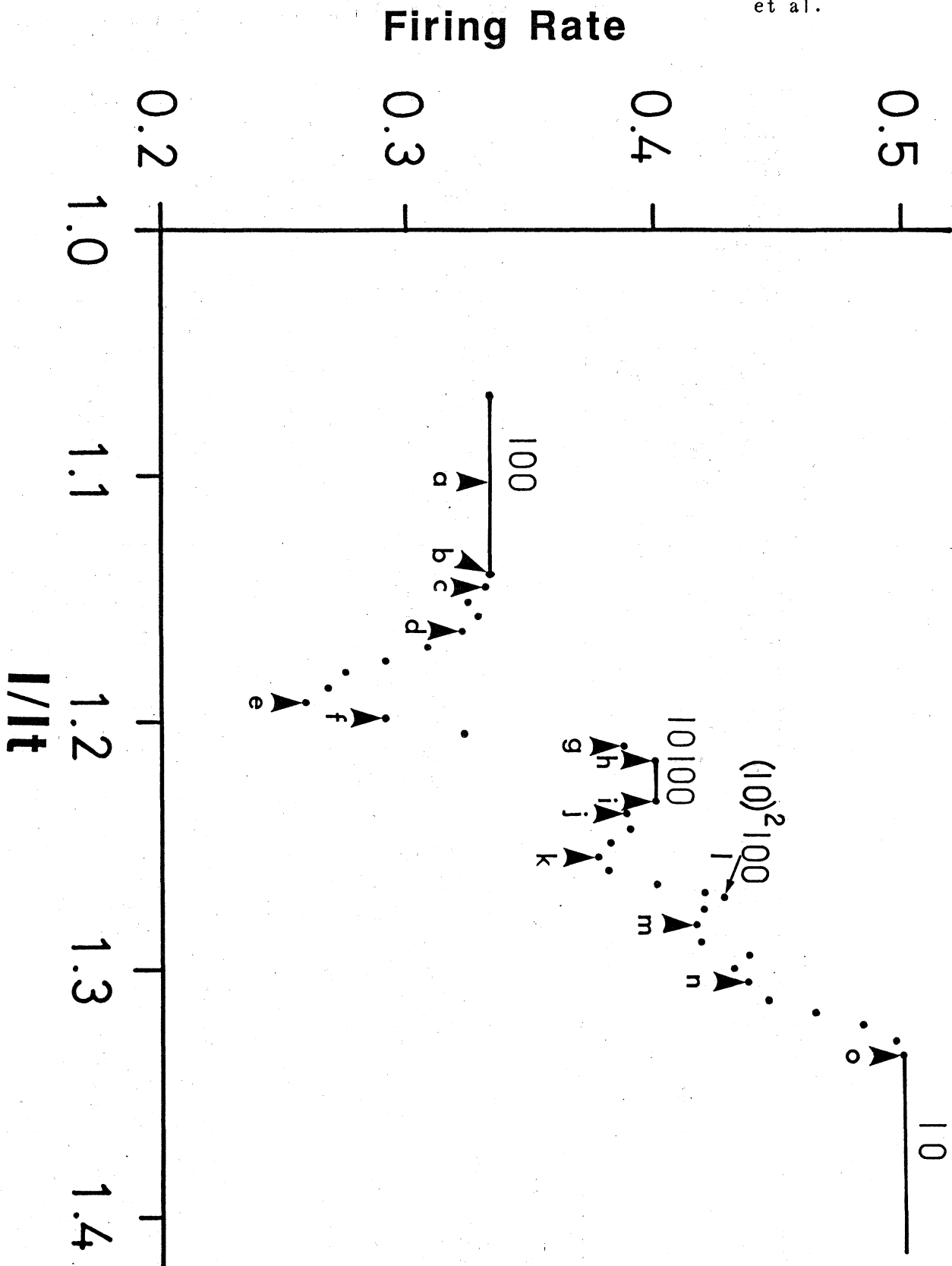


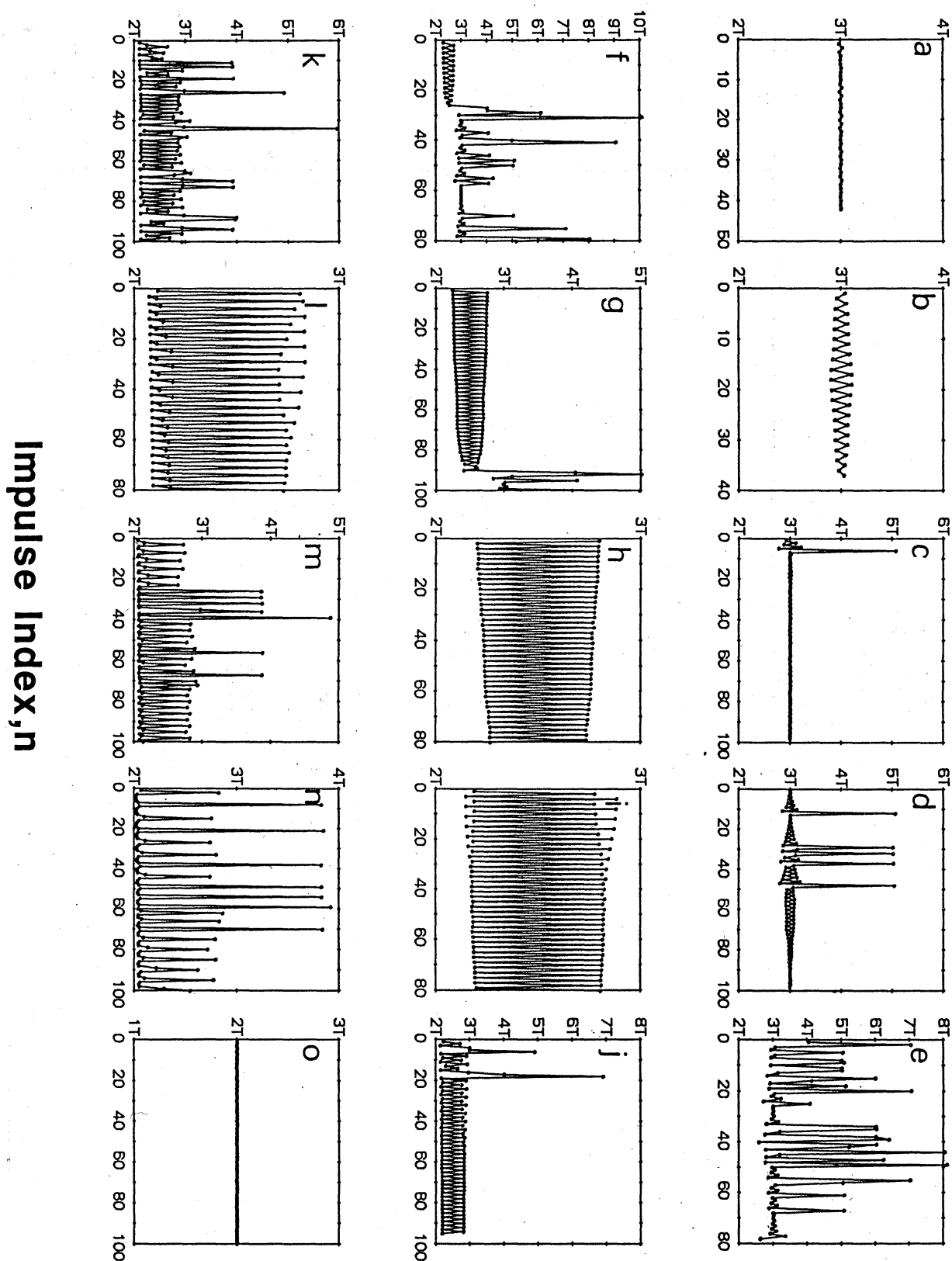
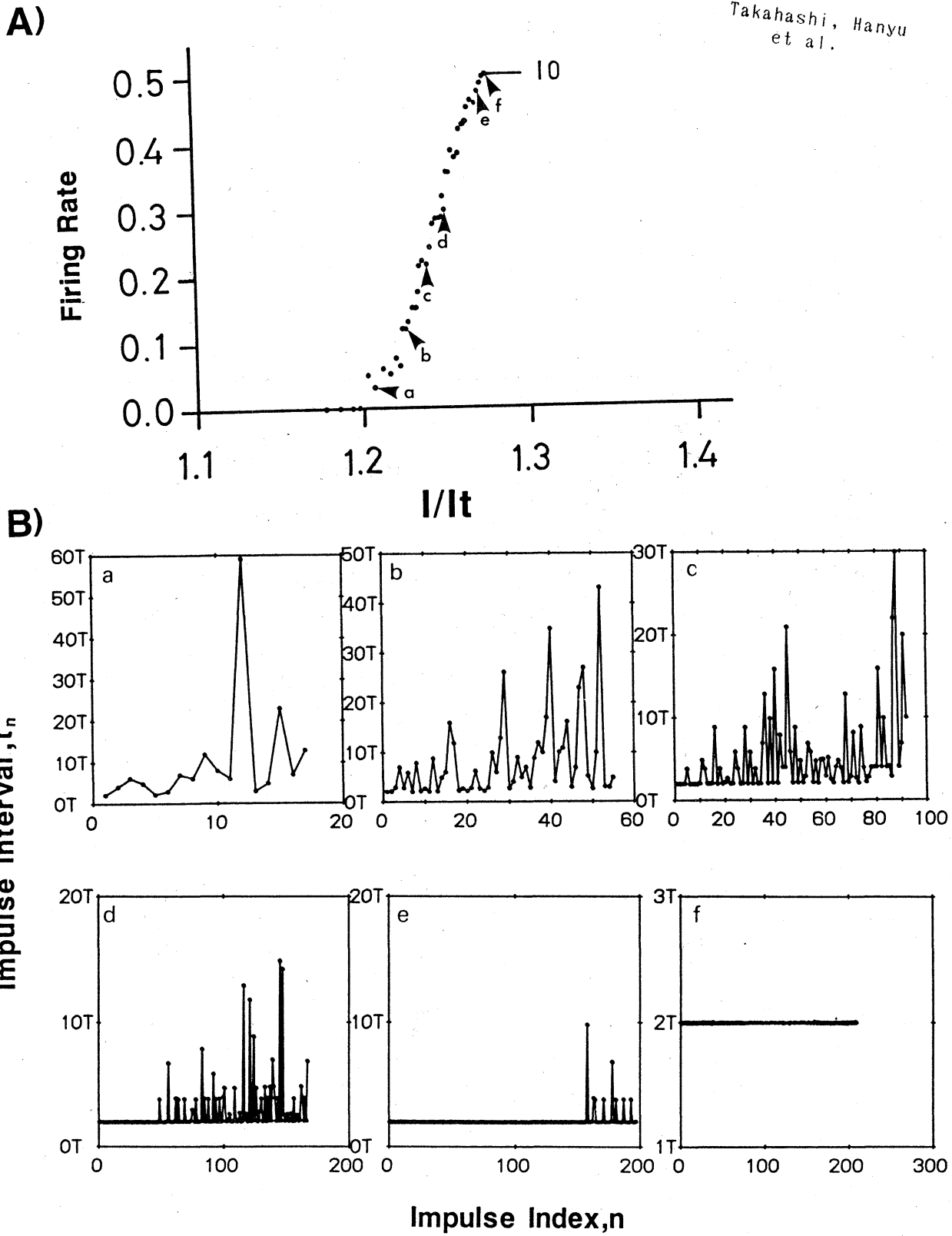
Fig.13
Takahashi, Hanyu
et al.

Fig.14
Takahashi, Hanyu
et al.



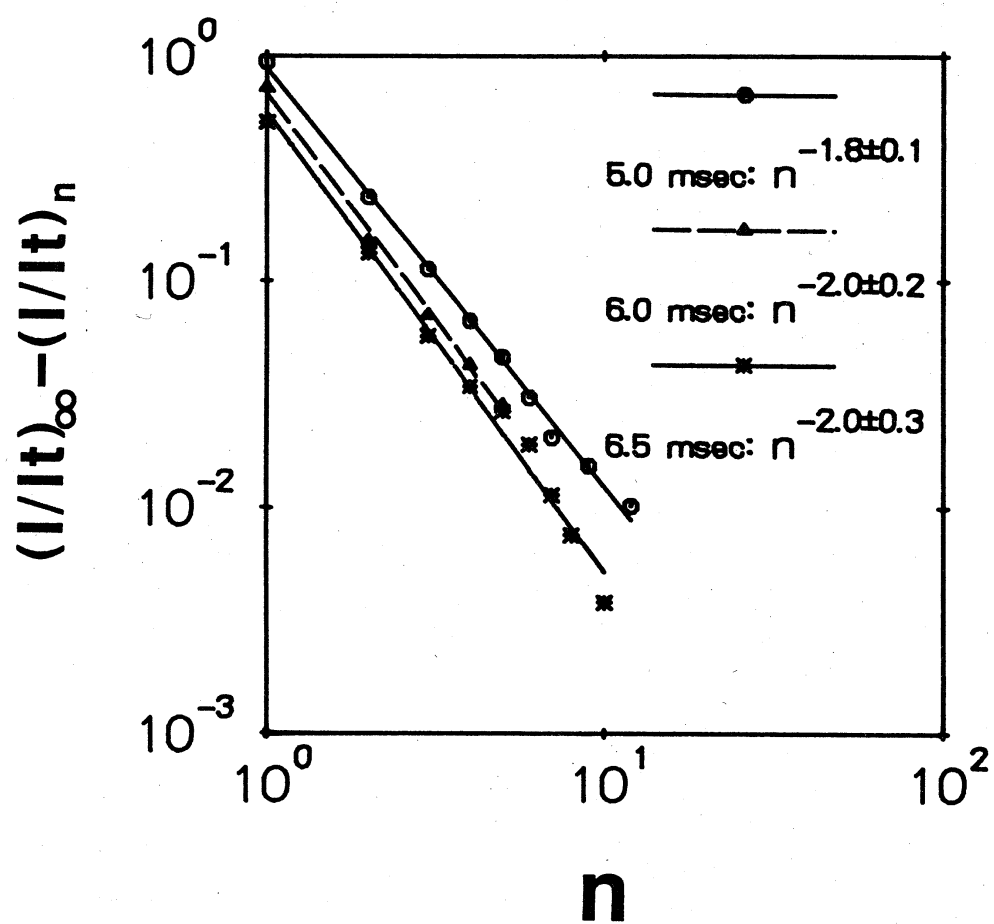


Fig.16
Takahashi, Hanyu
et al.

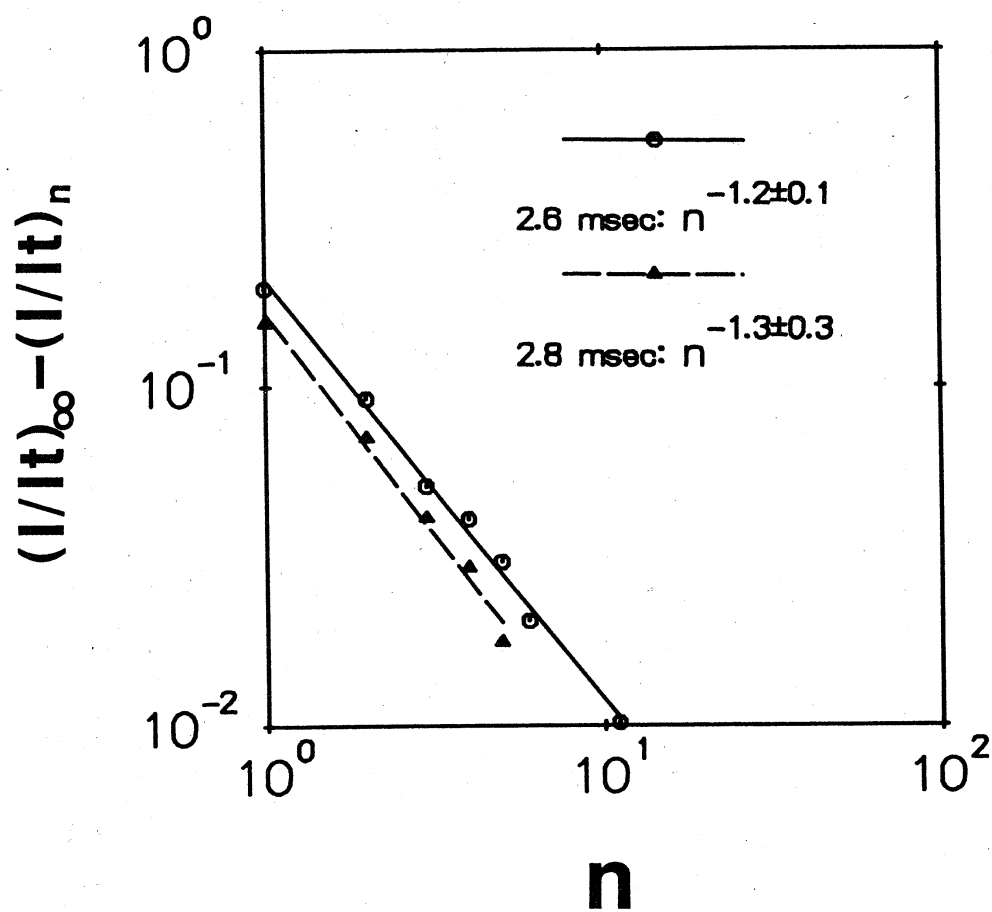


Fig.17
Takahashi, Hanyu
et al.

